

②

**U.S. ARMY INSTITUTE FOR RESEARCH  
IN MANAGEMENT INFORMATION,  
COMMUNICATIONS, AND COMPUTER SCIENCES  
(AIRMICS)**

**(ASQB-GC-90-019)**

**18 November 1989**

**115 O'Keefe Bldg  
Georgia Institute of Technology  
Atlanta, GA 30332-0800**

**91-01899**

91 6 11 177

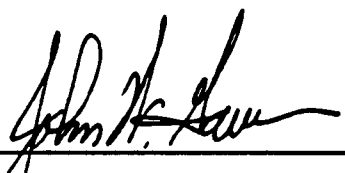
## REPORT DOCUMENTATION PAGE


Form Approved  
OMB No. 0704-0188  
Exp. Date: Jun 30, 1986

1a. REPORT SECURITY CLASSIFICATION <b>UNCLASSIFIED</b>			1b. RESTRICTIVE MARKINGS <b>NONE</b>	
2a. SECURITY CLASSIFICATION AUTHORITY <b>N/A</b>			3. DISTRIBUTION/AVAILABILITY OF REPORT  <b>N/A</b>	
2b. DECLASSIFICATION/DOWNGRADING SCHEDULE <b>N/A</b>				
4. PERFORMING ORGANIZATION REPORT NUMBER(S)			5. MONITORING ORGANIZATION REPORT NUMBER(S) <b>N/A</b>	
6a. NAME OF PERFORMING ORGANIZATION <b>AIRMICS</b>		6b. OFFICE SYMBOL (If applicable) <b>ASQB-GC</b>		7a. NAME OF MONITORING ORGANIZATION <b>N/A</b>
6c. ADDRESS (City, State, and Zip Code) <b>115 O'Keefe Bldg. Georgia Institute of Technology Atlanta, GA 30332-0800</b>			7b. ADDRESS (City, State, and ZIP Code) <b>N/A</b>	
8a. NAME OF FUNDING/SPONSORING ORGANIZATION <b>AIRMICS</b>		8b. OFFICE SYMBOL (If applicable) <b>ASQB-GC</b>		9. PROCUREMENT INSTRUMENT IDENTIFICATION NUMBER <b>N/A</b>
8c. ADDRESS (City, State, and ZIP Code) <b>115 O'Keefe Bldg. Georgia Institute of Technology Atlanta, GA 30332-0800</b>			10. SOURCE OF FUNDING NUMBERS	
			PROGRAM ELEMENT NO.	PROJECT NO.
			TASK NO.	WORK UNIT ACCESSION NO.
11. TITLE (Include Security Classification) <b>Performance Analysis of Hybrid ARQ Protocols in a Slotted Direct-Sequence Code-Division Multiple-Access Network: Jamming Analysis</b>				
12. PERSONAL AUTHOR(S) <b>LTC Joseph M. Hanratty</b>				
13a. TYPE OF REPORT <b>Research</b>		13b. TIME COVERED <b>FROM 11/88 TO 11/89</b>		14. DATE OF REPORT (Year, Month, Day) <b>89,11,18</b>
15. PAGE COUNT <b>57</b>				
16. SUPPLEMENTARY NOTATION				
17. COSATI CODES			18. SUBJECT TERMS (Continue on reverse if necessary and identify by block number) <b>Spread Spectrum Networks Code Division Multiple Access (CDMA) Automatic Repeat Request (ARQ) Hybrid ARQ</b>	
FIELD	GROUP	SUBGROUP		
19. ABSTRACT (Continue on reverse if necessary and identify by block number)  <b>This paper examines the performance of Type 1 Hybrid ARQ protocols in a slotted direct-sequence code-division multiple-access network operating in a hostile jamming environment. The network consists of an arbitrary number of transceivers arranged in a paired-off topology. The traffic arrival process is derived by means of a Markov model. Throughput-delay expressions are derived in terms of the channel cutoff rate and capacity. The effects of jammer state information are discussed. Network design parameters are identified and their dependency on system parameters is examined in detail. It is shown that, for a given population size, traffic intensity, and bit energy-to-jammer noise ratio, there is an optimal probability of retransmission, code rate, and processing gain that maximizes network performance in the presence of worst case jamming.</b>				
20. DISTRIBUTION/AVAILABILITY OF ABSTRACT <input checked="" type="checkbox"/> UNCLASSIFIED/UNLIMITED <input type="checkbox"/> SAME AS RPT. <input checked="" type="checkbox"/> DTIC USERS			21. ABSTRACT SECURITY CLASSIFICATION <b>Unclassified</b>	
22a. NAME OF RESPONSIBLE INDIVIDUAL <b>LTC Joseph M. Hanratty</b>			22b. TELEPHONE (Include Area Code) <b>(404) 894-3136</b>	22c. OFFICE SYMBOL <b>ASQB-GC</b>

This paper examines the performance of Type 1 Hybrid ARQ protocols in a slotted direct-sequence code-division multiple-access network operating in a hostile jamming environment. The network consists of an arbitrary number of transceivers arranged in a paired-off topology. The traffic arrival process is derived by means of a Markov model. Throughput-delay expressions are derived in terms of the channel cutoff rate and capacity. The effects of jammer state information are discussed. Network design parameters are identified and their dependency on system parameters is examined in detail. It is shown that, for a given population size, traffic intensity, and bit energy-to-jammer noise ratio, there is an optimal probability of retransmission, code rate, and processing gain that maximizes network performance in the presence of worst case jamming. This research report is not to be construed as an official Army position, unless so designated by other authorized documents. Material included herein is approved for public release, distribution unlimited. This material is protected by copyright laws.

**THIS REPORT HAS BEEN REVIEWED AND IS APPROVED**

S/   
John W. Gowens  
Division Chief  
CNSD

S/   
John R. Mitchell  
Director  
AIRMICS

**Performance Analysis of Hybrid ARQ Protocols  
in Slotted Direct-Sequence Code Division  
Multiple-Access Networks: Jamming Analysis**

**Joseph M. Hanratty**

**U. S. Army Institute for Research in Management Information,  
Communications, and Computer Sciences (AIRMICS)**

**Georgia Institute of Technology**

**Atlanta, Georgia 30332-0800**

**(404) 894-3136**

**Gordon L. Stüber**

**School of Electrical Engineering**

**Georgia Institute of Technology**

**Atlanta, Georgia 30332**

**(404) 894-2923**

### **Abstract**

This paper examines the performance of Type I Hybrid ARQ protocols in a slotted direct-sequence code division multiple-access network operating in a hostile jamming environment. The network consists of an arbitrary number of transceivers arranged in a paired-off topology. The traffic arrival process is derived by means of a Markov model. Throughput-delay expressions are derived in terms of the channel cut-off rate and capacity. The effects of jammer state information are discussed. Network design parameters are identified and their dependency on system parameters is examined in detail. It is shown that, for a given population size, traffic intensity, and bit energy-to-jammer noise ratio, there is an optimal probability of retransmission, code rate, and processing gain that maximises network performance in the presence of worst case pulse jamming.

## I Introduction

Code Division Multiple-Access (CDMA) is an attractive multiple accessing technique in packet radio networks because of its good signal capture, multiple-access, antimultipath, and narrowband interference rejection capabilities [1]. In a hostile jamming environment, CDMA may be necessary if any appreciable throughput is to be obtained.

Most of the early work in the area of spread spectrum multiple-access has been focused primarily on physical level issues such as spread spectrum format selection, spreading code design, and the corresponding bit error rate performance [2]. Analysis at the link level has been limited to investigating the effects of multiple-access interference and background noise for various network topologies [3,4,5,6,7]. Very few analyses have included the effects of jamming [6,8]. Within the framework of [6,7], this paper examines the performance of Type I Hybrid automatic-repeat request (ARQ) protocols [9] in a slotted direct-sequence CDMA network operating in a hostile jamming environment. The analysis in [7] considered the effects of multiple-access interference and background noise. In this paper, we obtain similar results while considering the effects of jamming.

Random access channel protocols such as slotted ALOHA are known to be more efficient than fixed access schemes such as TDMA and FDMA for bursty traffic. However, the throughput-delay performance for random access protocols decreases dramatically at high traffic loads. It was shown in [6,7] that, at high traffic intensities, it is more efficient in terms of network utilization to use CDMA in conjunction with random access than to use random access alone.

The key performance measures of random access networks are their throughput-delay characteristics. Hybrid ARQ schemes are often employed to improve the throughput-delay performance and to increase network reliability. The purpose of this paper is to evaluate and optimize the throughput-delay performance of Type I Hybrid ARQ protocols in a slotted direct-sequence CDMA network operating in a hostile jamming environment. Performance bounds are derived in terms of the channel cutoff rate and capacity. These bounds assume the use of error detecting/correcting codes operating arbitrarily close to the channel cutoff rate or capacity.

An overview of this paper is as follows. In section II, the network model is defined in terms of its physical and link level characteristics. The model accounts for the presence of multiple-access interference, background noise, and jammer noise. In section III, expressions are derived for the throughput and corresponding average packet delay in terms of the channel cutoff rate and capacity. Numerical results are presented in section IV to demonstrate the performance of the CDMA network. An extensive analysis is made to investigate the dependency of the throughput-delay performance on the choice of retransmission probability, code rate, and processing gain. The effect of traffic intensity, population size, and jammer noise level is considered in detail. The effect of background noise is included in the formulation, but not included in the numerical analysis because it is discussed in detail in [7]. Operational considerations are presented in section V.

## II Network and Channel Model

The network consists of  $2N$ ,  $1 < N < \infty$ , radio units arranged in a paired-off topology similar to that discussed in [6,7].  $N$  denotes the maximum possible number of active transmitter-receiver pairs during a given slot time. In the sequel,  $N$  is called the population size. The network operates in full-duplex mode, allowing for simultaneous packet transmission and reception. With a paired-off topology, each transmitter-receiver pair is assigned a unique spreading code. Whenever a transmitter is active, there is complete availability of its corresponding receiver. Therefore, the only disruptive interaction between concurrent packet transmissions is multiple-access interference, and the channel is not susceptible to the effects of capture.

Determining the impact of multiple-access interference in spread-spectrum network requires that we specify how the total interfering power is divided among the interfering signals. The analysis in this paper is applicable to a special class of networks where the probability distribution of the interference traffic is the same at each receiver, and each interferer contributes an equal amount to the total interfering power. All transmitters employ the same carrier frequency, code symbol duration  $T_s$ , modulation technique, processing gain  $\eta$ , and error detecting/correcting code. Furthermore, each receiver in the network is

assumed to be affected by the same jamming strategy. A practical example of such a network is the uplink of a satellite relay network, where the satellite has  $N$  receivers (one for each of  $N$  earth-based transmitters) and where the power received from each transmitter is about the same.

Transmitters access the channel by using direct-sequence CDMA with a standard slotted ALOHA protocol. Information is transmitted in the form of packets, one packet per time slot. Packet flow for the network is shown in Fig. 1. Each of the network's transmitters can be in one of two modes: origination or blocked. In the origination mode, the probability of transmitting a packet in the  $i^{\text{th}}$  future time slot is geometrically distributed with parameter  $p_o$ , where  $p_o$  is the probability that the transmitter will transmit the packet in the next time slot.

$$\text{Prob \{ packet transmission in the } i^{\text{th}} \text{ future time slot \}} = p_o(1 - p_o)^{i-1} \quad (1)$$

When either multiple-access interference, background noise, or jammer noise causes a packet to be received in error, a transmitter enters the blocked mode. In this mode, the probability of retransmitting a packet in the  $i^{\text{th}}$  future time slot is also geometrically distributed but with parameter  $p_r$ , where  $p_r$  is the probability that a transmitter will retransmit its packet in the next time slot. While a transmitter is waiting to retransmit, it is considered blocked or backlogged because it cannot transmit a new packet until the retransmitted packet is received without error. In practice, limits are set on the maximum number of retransmissions allowed for a given packet.

The traffic intensity is defined as the average number of packets transmitted per slot, and the new and retransmitted traffic intensities are denoted by  $\nu_o$  and  $\nu_r$ , respectively. At the input to the CDMA channel, new packet transmissions combine with packet retransmissions to form the composite channel traffic. The composite channel traffic can be characterized by its intensity and steady-state arrival distribution. The composite traffic intensity  $\nu$  simply equals the sum of the new and retransmitted traffic intensities ( $\nu = \nu_o + \nu_r$ ). The composite arrival distribution  $f_M(l)$  is the steady-state probability distribution for the number of attempted transmissions  $M$  in a given time slot. The form of this distribution depends primarily upon the relative values of  $p_o$  and  $p_r$ , and on the population size  $N$ .



Significant simplification in its form results when  $p_o = p_r = p$ , in which case the distribution becomes binomial with parameters  $p$  and  $N$ . Further simplification occurs when  $p_o = p_r \rightarrow 0$  and  $N \rightarrow \infty$ , in which case the binomial distribution approaches the Poisson distribution with arrival rate equal to the composite traffic intensity  $\nu$ .

A Type I Hybrid ARQ protocol is used for error control. This protocol combines the forward error detecting (FED) capability of plain (conventional) ARQ with the use of forward error correcting (FEC) codes to achieve improved network performance. The Type I Hybrid ARQ system under consideration is shown in Fig. 2. The ARQ portion of this protocol is of the stop-and-wait (SAW) variety, where the transmitter waits for either a positive (ACK) or negative (NACK) acknowledgement of the packet just transmitted before transmitting the next new or retransmitted packet, respectively. When a NACK is received, the transmitter retransmits the requested packet in the  $i^{th}$  future time slot with probability  $(1 - p_r)^{i-1} p_r$ . The FEC portion of the protocol is used to combat the effects of poor channel conditions and tends to reduce the number of retransmissions. Together, the proper combination of FEC and ARQ provide higher network reliability and throughput than could otherwise be achieved by them separately.

For this analysis, it is assumed that (N)ACKs are made over a separate return channel in the next immediate slot at no cost in performance. Cost free and completely reliable (N)ACKs are obtained by transmitting the one bit of acknowledgement information with a very large processing gain over a entire time slot. Large processing gains are used rather than optimal code rate-processing gain combinations. This allows (N)ACK packet power levels to be reduced so that their contribution to the multiple-access interference is negligible. Thus, (N)ACKs are assumed not to decrease network utilization.

Pulse jamming is an effective counter measure against direct-sequence spread-spectrum systems. For our purpose, the pulse jammer is modeled as having a two-level on-off power distribution. With probability  $\rho$ , a code symbol is jammed with additive white Gaussian noise (AWGN) having a one-sided power spectral density (PSD)  $N_J/\rho$ . With probability  $1 - \rho$ , a code symbol is unaffected by jamming. The average one-sided jammer noise PSD is  $N_J$ . For simplicity, it is assumed that a code symbol is either completely jammed or not

at all. Finally, the jammer is assumed to have complete knowledge of the multiple-access network except for the exact set of spreading sequences being used.

Each data packet that is transmitted over the Type I Hybrid ARQ system in Fig. 2 is comprised of one or more code words. Each code word is used for simultaneous error detection and error correction. Intrapacket interleaving is used to randomize the effects of pulse jamming, in an attempt to make the coding channel appear memoryless within a time slot. The coding channel is not memoryless from slot-to-slot because the multiple-access interference changes. When binary modulation is used, the code symbol error probability in the presence of AWGN is  $P_S = f(r\lambda_t)$  where  $r$  is the code rate and  $\lambda_t$  is the bit energy-to-total-noise ratio. For DPSK,  $f(r\lambda_t) = \frac{1}{2} \exp\{-r\lambda_t\}$ , and for BPSK  $f(r\lambda_t) = \text{erfc}(\sqrt{2r\lambda_t})$ . If we define  $b := r\lambda_t$  and  $a := \rho r\lambda_J$ , where  $\lambda_J$  is the bit energy-to-jammer noise ratio, then with probability  $1 - \rho$ ,  $P_S = f(b)$  and with probability  $\rho$ ,  $P_S = f(\frac{ab}{a+b})$ . For binary modulation with hard decision decoding, the coding channel is modeled as a binary symmetric channel (BSC) with crossover probability  $P_S$ , under the assumption of ideal interleaving.

The cutoff rate and the capacity of the BSC depends upon the availability of jammer state information. Without jammer state information, the cutoff rate and capacity are:

$$R_o = 1 - \log_2 \left( 1 + \sqrt{4P_S(1 - P_S)} \right), \quad (2)$$

$$C = 1 - H[P_S], \quad (3)$$

where  $H[P_S] = -P_S \log_2 P_S - (1 - P_S) \log_2 (1 - P_S)$  is the binary entropy function and

$$P_S = (1 - \rho)f(b) + \rho f\left(\frac{ab}{a+b}\right). \quad (4)$$

If jammer state information is available, then the BSC is comprised of two component channels;  $\Delta_1$ , when a code symbol is not jammed with probability  $1 - \rho$  and,  $\Delta_2$ , when a code symbol is jammed with probability  $\rho$ . The cutoff rate of  $\Delta_1$  is

$$R_{o,1} = 1 - \log_2 \left( 1 + \sqrt{4f(b)(1 - f(b))} \right), \quad (5)$$

and the cutoff rate of  $\Delta_2$  is

$$R_{o,2} = 1 - \log_2 \left( 1 + \sqrt{4f\left(\frac{ab}{a+b}\right)\left(1 - f\left(\frac{ab}{a+b}\right)\right)} \right). \quad (6)$$

The cutoff rate of the composite channel is [10]

$$R_o = -\log_2 E_S \left[ 2^{-R_o s} \right], \quad (7)$$

where the expectation is over the probability distribution of the component channels. The corresponding component channel capacities are

$$C_1 = 1 - H[f(b)], \quad C_2 = 1 - H \left[ f \left( \frac{ab}{a+b} \right) \right], \quad (8)$$

and the capacity of the composite channel is [10]

$$C = E_S[C_S] = 1 - H[f(b)] + \rho \left( 1 - H \left[ f \left( \frac{ab}{a+b} \right) \right] - 1 + H[f(b)] \right). \quad (9)$$

The particular CDMA technique considered in this study is spread spectrum multiple-access (SSMA) which, in the sequel, will generally be referred to as CDMA. SSMA is characterized by the use of high rate (many chips per code symbol) pseudonoise (PN) spreading sequences. Spreading code sequences are selected from code families having low off-peak autocorrelations and low cross-correlations. It is assumed that the period of the spreading sequences is much greater than the code symbol duration. Although well known sets of deterministic sequences are available (e.g., Gold codes), the analysis in this study assumes completely random spreading sequences. For direct-sequence SSMA, the multiple-access interference at the front end of the receiver matched to the desired signal can be modeled as additional broad-band Gaussian noise [11]. A rigorous justification of this Gaussian approximation via comparison with the exact error probabilities has been provided for deterministic sequences [12], and random sequences [13], under the assumption of coherent detection. Similar results for differentially coherent detection (DPSK) have been obtained [14].

Following the above Gaussian approximation, the equivalent one-sided noise PSD due to the  $i^{th}$  interferer is  $N_i = PT_C = E_S = rE_b$ , where  $P$  is the transmitted power,  $T_C$  is the PN chip duration,  $E_S$  is the code symbol energy, and  $E_b$  is the bit energy. The total additive noise at the front end of the  $n^{th}$  receiver is [15]

$$N_t = N_o + \eta^{-1} \sum_{\substack{j=1 \\ j \neq n}}^m rE_b, \quad (10)$$

where  $N_o$  is the background noise PSD,  $\eta = T_S/T_C$  is the processing gain, and  $m$  is the number of allowable simultaneous packet transmissions in a time slot. The bit energy-to-total noise ratio for the  $n^{th}$  receiver is

$$\lambda_t = \frac{E_b}{N_o + \eta^{-1} r E_b \sum_{\substack{j=1 \\ j \neq n}}^m} = \frac{\lambda_o}{1 + \eta^{-1} r \lambda_o (m - 1)}, \quad (11)$$

where  $\lambda_o$  is the bit energy-to-background noise ratio.

### III Network Analysis

In this section, expressions for the throughput and corresponding average packet delay are derived in terms of the channel cutoff rate and capacity. The impact of jammer state information is considered.

#### III-A Throughput Analysis

The throughput  $T$  at the output of our CDMA system is defined as the expected number of successful packets  $S$  per slot;

$$T = E[S]. \quad (12)$$

The throughput can also be expressed as [7]

$$T = \sum_{l=1}^N l P_C(l) f_M(l), \quad (13)$$

where  $f_M(l)$  is the probability distribution function for the number of attempted transmissions (composite arrivals) during a particular slot interval and  $P_C(l)$  is the probability of a correctly received packet when there are  $l$  simultaneous packet transmissions.

The composite packet arrival distribution  $f_M(l)$  is derived in [3,7] by using a Markov model for the number of backlogged transmitters. The channel is viewed as a discrete-time system where the number of backlogged transmitters  $X(t)$  represents a Markov process with state transition matrix  $\mathbf{P} = [p_{ij}]$ . State transition probabilities  $p_{ij}$  are defined as the probability of moving from a state having  $i$  backlogged transmitters in time slot  $t$  to a state

having  $j$  backlogged transmitters in time slot  $t + 1$  or

$$p_{ij} = \text{Prob}\{X(t+1) = j \mid X(t) = i\}. \quad (14)$$

Expressions for the  $p_{ij}$ 's are developed in [7]. With  $\mathbf{P}$ , we can solve for the equilibrium state probability distribution for the number of backlogged transmitters  $\pi$  in the following equation:

$$\pi = \pi \mathbf{P}, \quad (15)$$

where

$$\pi = [\pi(0), \pi(1), \dots, \pi(N)], \quad \sum_{n=0}^N \pi(n) = 1. \quad (16)$$

#### No Jammer State Information

The throughput in the presence of jamming is dependent upon the availability of jammer state information. Jammer state information will increase throughput by increasing the cutoff rate and capacity of the coding channel. First, consider the case of no jammer state information. Observe from (2) and (3) that  $R_o$  and  $C$  can be expressed in the form  $R_o = g_{R_o}(P_S)$  and  $C = g_C(P_S)$ , respectively. For convenience, these functions can be expressed in the union form  $\{R_o, C\} = g_{\{R_o, C\}}(P_S)$ . Likewise, these functions can be inverted to obtain expression for the probability of symbol error as a function of the cutoff rate and capacity,  $P_S = g_{\{R_o, C\}}^{-1}(R_o, C)$ . For the cutoff rate,

$$P_S = \frac{(1 - \sqrt{1 - \alpha^2})}{2}, \quad \alpha = 2^{1-R_o} - 1, \quad (17)$$

and for the capacity

$$P_S = H^{-1}[1 - C], \quad (18)$$

where  $H^{-1}(\cdot)$  is the inverse binary entropy function. By equating (4) and (17, 18), and recalling that  $a := \rho r \lambda_J$  and  $b := r \lambda_i$ , the following expression can be obtained for the bit energy-to-jammer noise ratio;

$$\lambda_J = \frac{a(f(\frac{ab}{a+b}) - f(b))}{r(g_{\{R_o, C\}}^{-1}(R_o, C) - f(b))}. \quad (19)$$

Substituting (11) into (19) and rearranging gives the following expression;

$$g_{\{R_o, C\}}^{-1}(R_o, C) + \left( \frac{a}{\lambda_J r} - 1 \right) f \left( \frac{r \lambda_o}{1 + \eta^{-1} r \lambda_o (m - 1)} \right) - \frac{a}{\lambda_J r} f \left( \frac{a r \lambda_o}{a[1 + \eta^{-1} r \lambda_o (m - 1)] + r \lambda_o} \right) = 0 \quad (20)$$

The objective of the pulse jammer is to minimize the throughput for a given  $p_r$ ,  $r$ ,  $\eta$ ,  $\lambda_o$ , and  $\lambda_J$ . Therefore, a worst case pulse jammer chooses  $a$  so that  $m$  in (20) is minimized.

If the optimal jamming fraction is unity, which usually occurs for sufficiently low code rates, then (19) reduces to

$$\lambda_J = \frac{\lambda_t f^{-1}(g_{\{R_o, C\}}^{-1}(R_o, C))}{r \lambda_t - f^{-1}(g_{\{R_o, C\}}^{-1}(R_o, C))}, \quad (21)$$

where  $f^{-1}(\cdot)$  is the inverse operator of  $f(\cdot)$ . By using (11) and (21), the following expression can be obtained for the number of allowable simultaneous packet transmissions in a time slot;

$$m = \frac{\eta}{r} \left( \frac{r}{f^{-1}(g_{\{R_o, C\}}^{-1}(R_o, C))} - \frac{1}{\lambda_o} - \frac{1}{\lambda_J} \right) + 1. \quad (22)$$

As in [6,7], suppose that the code being used has the property that the packet error probability is zero if  $r \leq C$  and one if  $r > C$ . This ideal threshold effect occurs because it is possible to achieve arbitrarily reliable communication for all code rates up to channel capacity, while it is impossible to achieve reliable communication with a code having a rate exceeding capacity. In practice, it is extremely difficult to operate with a code rate near capacity. The cutoff rate  $R_o$  has been proposed by Massey [16], and others, as a more realistic upper bound on the achievable rate. For sequential decoding of convolutional codes,  $R_o$  is the computational cutoff rate, and is usually viewed as the practical limit on the highest rate at which a sequential decoder can operate. If  $r > R_o$ , then frequent buffer overflows occur resulting in many decoding errors. On the other hand, it has been demonstrated that it is possible to operate very close to the cutoff rate. In [17], for example, two constraint length 21 rate 4/5 convolutional codes were used over a channel such that  $r = 0.988 R_o$ . In 1000 packets, each consisting of 1000 bits, there were no observed decoding errors. As the constraint length of the code and/or the buffer size in the

sequential decoder is increased, this threshold effect becomes even more pronounced [18]. Stüber [19] evaluated a Layland Lushbaugh constraint length 32 rate  $\frac{1}{2}$  convolutional code [20], where Fano sequential decoding was used under a time out condition. The computer simulation consisted of transmitting 400 packets, each consisting of  $L = 1000$  bits, over a BSC. The decoder used hard decision decoding without channel state information. The probability of correct packet reception was obtained as a function of the channel crossover probability for various time out limits. It was shown that the ideal decoder threshold approximation is quite accurate in terms of the network optimization, for convolutionally encoded packets with a Fano sequential decoder. Thus, for our purpose, an ideal decoder threshold is assumed, where the packet error probability is zero if  $r \leq R_o$  and one if  $r > R_o$ . Results derived under the assumption of an ideal decoder threshold at capacity are included for comparison purposes.

Now consider the limiting case as  $r \rightarrow \{R_o, C\}$  and suppose that the values of  $N$ ,  $\{R_o, C\}$ ,  $\eta$ ,  $\lambda_o$ , and  $\lambda_J$  are fixed. If the optimal  $\rho$  is unity, then (22) gives the maximum number of allowable simultaneous packet transmissions as  $\hat{m} = \lfloor m \rfloor$ . If the actual number of packets  $l$  exceeds  $\hat{m}$ , then information is being transmitted at a rate above the cutoff rate or capacity of the channel. As a result, all packets are incorrectly received and must be retransmitted ( $P_C(l) = 0, l > \hat{m}$ ). If the number of packets is less than or equal to  $\hat{m}$ , then all packets are received successfully ( $P_C(l) = 1, l \leq \hat{m}$ ). The throughput expression in (13) becomes

$$T = \sum_{l=1}^{\min(\hat{m}, N)} l f_M(l). \quad (23)$$

In order to compare throughputs of different systems on an equal basis, we need to account for  $\{R_o, C\}$  and  $\eta$ . The normalized throughput or network utilization becomes

$$T(p_r, \{R_o, C\}, \eta, \rho) = \frac{\{R_o, C\}}{\eta} T = \frac{\{R_o, C\}}{\eta} \sum_{l=1}^{\min(\hat{m}, N)} l f_M(l). \quad (24)$$

This is the average number of successful packets (per slot) per unit time per unit bandwidth. Note that the normalized throughput is a function of the probability of retransmission, the code rate, the processing gain, the jamming fraction, and is always less than one. The normalized throughput is also a function of the population size, the composite traffic

intensity, the bit energy-to-background noise ratio, and the bit energy-to-jammer noise ratio. However, this dependency is not shown explicitly because these parameters are assumed to be uncontrolled. The maximin normalized throughput is

$$\begin{aligned} T_{\{R_o, C\}} &= \max_{0 < p_r \leq 1} \max_{\substack{0 < \{R_o, C\} \leq 1 \\ 1 \leq \eta}} \min_{0 < \rho \leq 1} T(p_r, \{R_o, C\}, \eta), \\ &= \max_{0 < p_r \leq 1} \max_{\substack{0 < \{R_o, C\} \leq 1 \\ 1 \leq \eta}} \min_{0 < \rho \leq 1} \frac{\{R_o, C\}}{\eta} \sum_{l=1}^{\min(m, N)} l f_M(l). \end{aligned} \quad (25)$$

For the cutoff rate case, (25) represents the practically achievable limit on the maximin normalized throughput  $T_{R_o}$ . For the capacity case, (25) represents the theoretical upper limit on the maximin normalized throughput,  $T_C$ . The optimal probability of retransmission, code rate, processing gain, and jamming fraction are denoted by  $p_r^*$ ,  $\{R_o^*, C^*\}$ ,  $\eta^{\{R_o, C\}}$ , and  $\rho^{\{R_o, C\}}$ , respectively.

#### Jammer State Information

If jammer state information is available, it is expected that throughput can be increased. In this case, expressions for the bit energy-to-jammer noise ratio can be obtained by performing the expectations in (7) and (9) and manipulating the results. For the cutoff rate case, the following expression can be obtained;

$$\lambda_J = \frac{2a \left( \sqrt{f\left(\frac{ab}{a+b}\right) \left(1 - f\left(\frac{ab}{a+b}\right)\right)} - \sqrt{f(b)(1 - f(b))} \right)}{r \left( \alpha - \sqrt{4f(b)(1 - f(b))} \right)} \quad (26)$$

Substituting  $a = \rho R_o \lambda_J$  and  $b = R_o \lambda_t$  into (26) results in

$$\begin{aligned} \lambda_J R_o \left( \alpha - \sqrt{4f(R_o \lambda_t)(1 - f(R_o \lambda_t))} \right) = \\ 2a \left( \sqrt{f\left(\frac{a R_o \lambda_t}{a + R_o \lambda_t}\right) \left(1 - f\left(\frac{a R_o \lambda_t}{a + R_o \lambda_t}\right)\right)} - \sqrt{f(R_o \lambda_t)(1 - f(R_o \lambda_t))} \right) \end{aligned} \quad (27)$$

where  $\lambda_t$  is given by (11). Once again, a pulse jammer chooses  $a$  in (27) so that  $m$  is minimized.

If the optimal jamming fraction  $\rho$  is unity, then  $a = r \lambda_J$  and (26) reduces to (19). For a given  $N$ ,  $r = R_o$ ,  $\eta$ ,  $\lambda_o$ , and  $\lambda_J$ , this gives the same  $m$  (22) that would result if the receiver did not have jammer state information. This makes sense because when  $\rho = 1$



the coding channel is comprised of only one component coding channel. Once again, the maximin normalized throughput is given by (25) with  $\hat{m} = \lfloor m \rfloor$ .

For the capacity case, the following expression for the bit energy-to-jammer noise ratio can be obtained;

$$\lambda_J = \frac{a \left( H[f(b)] - H \left[ f \left( \frac{ab}{a+b} \right) \right] \right)}{r(C + H[f(b)] - 1)}. \quad (28)$$

By using  $b = C\lambda_t$  and (11) in (28),  $m$  satisfies

$$1 - C + \left( \frac{a}{\lambda_J r} - 1 \right) H \left[ f \left( \frac{r\lambda_o}{1 + \eta^{-1} r\lambda_o(m-1)} \right) \right] - \frac{a}{\lambda_J r} H \left[ f \left( \frac{ar\lambda_o}{a[1 + \eta^{-1} r\lambda_o(m-1)] + r\lambda_o} \right) \right] = 0. \quad (29)$$

As earlier, the jammer chooses  $\rho$  to minimize  $m$  in (29). If  $\rho = 1$ , then the coding channel consists of one state and the expression in (22) gives the value of  $m$ . The maximin normalized throughput is given by (25) with  $\hat{m} = \lfloor m \rfloor$ .

### III-B Delay Analysis

The average packet delay  $D$  of a network is often modeled as the sum of a random delay component  $D_r$ , a deterministic component  $D_d$ , and a one slot transmission time;

$$D = D_r + D_d + 1. \quad (30)$$

The deterministic component  $D_d$  can be used to model any fixed delay inherent in the network. For this analysis, it is assumed that the deterministic component is zero. As such, equation (30) becomes

$$D = D_r + 1. \quad (31)$$

The random delay component  $D_r$  is the average retransmission delay defined as

$$D_r = \frac{E}{p_r}, \quad (32)$$

where  $E$  is the average number of packet retransmissions per successfully transmitted packet. This delay represents the average rescheduling delay or the average backlog time experienced by a transmitter. This random component is necessary to prevent backlogged

transmitters from contending with other transmitters blocked during the same time slot. From Little's result [21],  $D_r$  can be expressed as

$$D_r = \frac{\bar{n}}{T_{\{R_o, C\}}}, \quad (33)$$

where  $\bar{n}$  is the average number of backlogged transmitters which can be calculated from

$$\bar{n} = \sum_{n=0}^N n\pi(n). \quad (34)$$

By using (31) and (33), the throughput can be directly related to the average packet delay (30) as

$$T_{\{R_o, C\}} = \frac{\bar{n}}{D - 1}. \quad (35)$$

Throughput can also be related to  $E$  by the following expression

$$E = \frac{\nu}{T_{\{R_o, C\}}} - 1, \quad (36)$$

where  $\nu/T_{\{R_o, C\}}$  is the average number of times a packet must be transmitted until it is successfully received. Substituting (36) and (33) into (32), the probability of retransmission can be expressed as

$$p_r = \frac{\nu - T_{\{R_o, C\}}}{\bar{n}}. \quad (37)$$

A similar expression for the probability of original packet transmission can be obtained as

$$p_o = \frac{\nu_o}{\sum_{n=1}^N (N - n)\pi(n)} = \frac{T}{N - \bar{n}}. \quad (38)$$

These expressions for  $p_r$  and  $p_o$  are used in computing the  $\mathbf{P}$  matrix (15) and are key in performing the optimization in (25).

## IV Performance Evaluation

In this section, the dependency of the network's throughput-delay performance on  $N$ ,  $\nu$ ,  $\lambda_J$ ,  $p_r$ ,  $\{R_o, C\}$ ,  $\eta$  and  $\rho$  is examined in detail, under the assumption of DS/DPSK signaling. The dependency of  $p_r$ ,  $\{R_o^*, C^*\}$ ,  $\eta^{\{R_o, C\}}$ , and  $\rho^{\{R_o, C\}}$  on  $N$ ,  $\nu$ , and  $\lambda_J$  is discussed. The effect of jammer state information is also considered. Throughout the analysis, background noise is neglected in order to isolate the effects of jamming. The effects of background noise are considered in [7].

#### IV-A Throughput-Delay Performance

Figs. 3-4 are plots of the maximin normalized throughput,  $T_{\{R_o, C\}}$  against the traffic intensity  $\nu$ . Figs. 5-8 are plots of  $T_{\{R_o, C\}}$  against average packet delay  $D$ . These plots illustrate the combined effects of maximizing throughput over probability of retransmission  $p_r$ , code rate  $\{R_o, C\}$ , and processing gain  $\eta$ , while minimizing the throughput over the jamming fraction  $\rho$ . The first maximization required by (25) is performed for a given level of jammer noise by fixing  $D$  in (35), allowing  $p_r$  to vary ( $0 \leq p_r \leq 1$ ) in (15), and solving for a  $(\bar{n}, \pi(n))$  solution which maximizes the throughput (35). Note that the usual bursty user assumption ( $p_r > p_o$ ) is relaxed, and that most of the throughput-delay results reported below require that  $p_o > p_r$ . This procedure is repeated for all possible values of  $\hat{m}$  ( $1 \leq \hat{m} \leq N$ ) and results in  $N$  optimal  $(p_r, T_{\{R_o, C\}})$  pairs for each fixed value of  $D$ . An alternate procedure, whereby the throughput is fixed and the delay is minimized, produces the same optimal  $(p_r, T_{\{R_o, C\}}, \hat{m}, D)$  combinations. For the second maximization required by (25),  $D$  is again fixed for a given level of jammer noise, and the code rate and processing gain  $\{R_o, C; \eta\}$  are allowed to vary. For each code rate-processing gain combination, the final step of the optimization is performed by allowing  $a = \rho r \lambda_j$  to vary in order to obtain a minimum value of  $m$  (i.e., the jammer has the final say). The last two steps of the optimization yield  $\hat{m}$  values for which the corresponding throughputs are known from step one. Each value of throughput is then normalized and the maximin normalized value is selected.

Two cases are considered for the jamming analysis. The first case assumes that  $\lambda_j$  is constant, regardless of the processing gain. This means that the jammer will offset any relative increase in the processing gain, by increasing its total power by the same relative amount. Therefore, an increase in the processing gain only reduces the effect of multiple-access interference. We consider this case because it provides some insights into the behavior of the network that would otherwise go unnoticed.

The second case is more realistic, because it assumes that the total jammer power is constant. Therefore, if the spread-spectrum bandwidth is extended by a relative increase in the processing gain, then the average bit energy-to-jammer noise ratio will be increased by the same relative amount. Consequently, an increase in the processing gain reduces both

the effects of multiple-access interference and jamming. For this case we define  $\tilde{\lambda}_J$  as the bit energy-to-jammer noise ratio that would be obtained with unity processing gain, i.e.,  $\tilde{\lambda}_J = \lambda_J |_{\eta=1}$ . With constant jamming power,  $\tilde{\lambda}_J$  is also constant. Then if  $\eta > 1$ , the bit energy-to-jammer noise ratio will be  $\lambda_J = \eta \tilde{\lambda}_J$ . Therefore, the optimization in (25) is performed in exactly the same manner as in the constant  $\lambda_J$  analysis except that  $\lambda_J = \eta \tilde{\lambda}_J$ .

#### IV-A.1 Optimization of Throughput-Delay Performance Over Probability of Retransmission

Values of optimal retransmission probability  $p_r^*$  exist for all values of traffic intensity as shown in Fig. 9. Note that the  $p_r^*$  values depend only on population size and traffic intensity and do not directly depend on the background and jammer noise levels. For the low range of traffic intensities ( $\nu < 1.0$ ), there are two distinct  $p_r^*$  values for each value of  $\nu$ . Selecting the lower  $p_r^*$  value for a given traffic intensity results in the maximum possible value for  $T_{\{R_o, C\}}$  (Figs. 3-4) but with nonminimal delay (Figs. 5-8). In Figs. 5-8, these lower  $p_r^*$  values correspond to the upper branch of the throughput-delay curve. Here,  $\nu$  is increasing along the curve from A to B and back to C. Points on the A-B portion of the curve correspond to stable operating points, whereas those on the B-C portion of the curve do not. A maximal  $T_{\{R_o, C\}}$  value is achieved under the following conditions:  $p_r^* \ll 1.0$ ,  $p_o \rightarrow 1.0$ , and  $\bar{n} \rightarrow N$ . As a result, the throughput is closely approximated by the equation  $T_{\{R_o, C\}} = \nu$  for low  $\nu$  ( $\nu < 0.5$ ) in Figs. 3-4, and by the equation  $T_{\{R_o, C\}} = N/D$  for the upper branch (A-B) in Figs. 5-8. These two throughput expressions are related through Little's result (33) by applying the above conditions to (37) and (35), respectively.

Selecting the higher  $p_r^*$  value for a given traffic intensity ( $\nu < 1.0$ ) in Fig. 9 results in a nonmaximal  $T_{\{R_o, C\}}$  value (not shown in Figs. 3-4) but at minimal delay (Figs. 5-8). The higher  $p_r^*$  values correspond to the lower right-hand branch of the throughput-delay curve in Figs. 5-8 (increasing  $\nu$  from E to F). This throughput-delay curve agrees with the results from earlier throughput-delay analyses for conventional narrow-band slotted ALOHA [22]. For these nonmaximal  $T_{\{R_o, C\}}$  values,  $p_r^* > p_o$  and  $\bar{n}$  is relatively low.

Note in Fig. 9 that for the low range of traffic intensities ( $\nu < 1.0$ ), the upper and

lower curves for  $p_r^*$  are separate and distinct. For a given traffic intensity, this separation represents the change in  $p_r^*$  that is necessary to move the network from an operating point having maximal throughput to one having minimal delay, and vice-versa. In Fig. 5, for example, the throughput-delay points for traffic intensities of  $\nu = 0.525$  and  $1.00$  are plotted for comparison purposes for the two values of  $p_r^*$ . Note in this example, that for  $\nu = 1.0$  it seems that an improvement in throughput can be had for a modest increase in delay by operating on the upper branch (B-C). However, the upper branch (B-C) operating point is not stable, whereas, the lower branch (E-F) operating point is stable. Similar statements can also be made for channels with background noise [7].

For the upper range of traffic intensities ( $\nu > 1.0$ ) in Fig. 9, there are also two possible optimal values for the probability of retransmission  $p_r^*$  as indicated by the solid and dashed lines. The solid line corresponds to the case when either plain or Hybrid ARQ is the optimal protocol. Here,  $p_r^*$  can be approximated by  $p_r^* = \nu/N$ . Because  $p_r^*$  is independent of  $\lambda_J$ , the same value of  $p_r^*$  is used for both plain and Hybrid ARQ for a given traffic intensity. The dashed line corresponds to the case when Type 1 Hybrid ARQ with CDMA (hereafter referred to as CDMA) is used. Here,  $p_r^* = \nu/N$  exactly and the composite arrival distribution  $f_M(l)$  is binomial. Note in Fig. 9 that the (dashed)  $p_r^* = \nu/N$  lines are shown for their widest possible range of values. Where they actually begin (lower left end) depends on the cutoff intensity (discussed below) which, in turn, depends on  $\lambda_J$ . Where the dashed lines end (upper right end) depends on the population size and the traffic intensity. At high intensity, high processing gain causes  $\hat{m} = N$ . As a result, there are no packets to retransmit and the  $p_r^* = \nu/N$  lines terminate. Also, at very high traffic intensities, the  $p_r = \nu/N$  relationship is no longer exact, but remains a good approximation [23].

#### IV-A.2 Throughput-Delay Performance at Constant Bit Energy-to-Jammer Noise Ratio

Figs. 3-4 and 5-8 are plots of maximin normalized throughput,  $T_{\{R,C\}}$ , against traffic intensity  $\nu$  and against average delay  $D$ , respectively. Results are shown for population sizes  $N = 10$  and  $30$  and for constant bit energy-to-jammer noise levels of  $\lambda_J = \infty$  and

$\lambda_J = 10.00$  dB. When jamming is present the effect of jammer state information is shown. Note that for the plain/Hybrid ARQ case, throughput becomes vanishingly small and delay becomes unbounded as the traffic intensity increases. However, when CDMA is used, this degradation in performance does not occur. Instead, the maximum normalized throughput (Figs. 3-4) decreases to some minimal value, at a particular traffic intensity, and then increases again. The corresponding delay decreases (Figs. 5-8). The traffic intensity at which CDMA achieves this improved performance over plain/Hybrid ARQ is defined as the *cutoff traffic intensity* which is denoted as  $\nu^{\{R_o, C\}}$  and is described as follows. If  $\nu < \nu^{\{R_o, C\}}$ , then the optimal processing gain  $\eta^{\{R_o, C\}}$  is unity for all bit energy-to-jammer noise ratios ( $\lambda_J \leq \infty$ ). If  $\nu > \nu^{\{R_o, C\}}$ , then  $\eta^{\{R_o, C\}} > 1$  with the actual value depending on the traffic intensity, population size, and the bit energy-to-jammer noise ratio. In Figs. 3-4, the cutoff intensities occur at the intersection of the CDMA curves with the plain/Hybrid ARQ curves. In Figs. 5-8, point C is an example of a throughput-delay point which corresponds to a cutoff intensity. Note how the delay drops precipitously (C-D) when CDMA is used. Recall that the above throughput-delay results must be adjusted for any fixed delay inherent in the particular network being considered. Additional fixed delay causes the curves in Figs. 5-8 to be shifted upward by a corresponding amount.

The throughput-delay curves of Figs. 5-8 represent a bounded region of operation where throughput and delay may be traded-off between one another. For example, unit delay  $D = 1.0$  can be achieved with CDMA for the entire range of traffic intensities by selecting the appropriate code rate and processing gain combination so that  $\hat{m} = N$ . In most cases, however, unit delay is achieved at the expense of a far from optimal throughput. Unit delay curves are shown in Fig. 3 for the cutoff rate and capacity cases at  $\lambda_J = \infty$ . In general, the throughput at unit delay  $T_{D=1}$  is very small for  $0 < \nu < \nu^{\{R_o, C\}}$ . At  $\nu = \nu^{\{R_o, C\}}$ , there is a step increase in  $T_{D=1}$ , after which  $T_{D=1} \rightarrow T_{\{R_o, C\}}$  as  $\nu \rightarrow N$ .

Figs. 10-11 illustrate the effect of bit energy-to-jammer noise ratio  $\lambda_J$ , population size  $N$ , and jammer state information on the cutoff traffic intensity  $\nu^{\{R_o, C\}}$ . In general,  $\nu^{\{R_o, C\}}$  increases to its maximum value ( $N$ ) as  $\lambda_J$  decreases. Note that for each  $\nu^{\{R_o, C\}}$  there is a corresponding  $\lambda_J$  which is defined as the *jammer noise limit* for that cutoff intensity,

denoted by  $\lambda_J^{\{R_o, C\}}$ . Also, for each  $\lambda_J$  there is a corresponding cutoff traffic intensity. The  $\lambda_J$  which  $\nu^{\{R_o, C\}}$  is asymptotic to is defined as the network *asymptotic jammer noise limit*, and is denoted  $\hat{\lambda}_J^{\{R_o, C\}}$ . With jammer state information,  $\hat{\lambda}_J^{\{R_o, C\}} = \{6.82 \text{ dB}, 4.81 \text{ dB}\}$ . Without jammer state information,  $\hat{\lambda}_J^{\{R_o, C\}} = \{7.39 \text{ dB}, 4.97 \text{ dB}\}$ . The network cannot operate at bit energy-to-jammer noise ratios below these asymptotic jammer noise limits, because they represent the smallest  $\lambda_J$  that can be present for reliable coded communication in the absence of multiple-access interference [6].

Figs. 12-13 show how the optimal processing gain  $\eta^{\{R_o, C\}}$  depends on the traffic intensity for various population sizes  $N$ , bit energy-to-jammer noise ratios  $\lambda_J$ , and jammer state availability. For the  $N = \infty$  case,  $\eta^{\{R_o, C\}}$  depends on  $\nu$  in a nearly linear fashion. The effect of finite population size is a 'staircase' type curve which tends to the  $N = \infty$  curve as  $N \rightarrow \infty$ . Note that for the cutoff rate case, systems with jammer state information require larger values of  $\eta^{R_o}$  than those without jammer state information, while for the capacity case, jammer state information has no impact at  $\lambda_J = 10.00 \text{ dB}$  because  $\rho^C = 1$ .

Figs. 14-15 show how the optimal processing gain  $\eta^{\{R_o, C\}}$  depends on the bit energy-to-jammer noise ratio  $\lambda_J$  for a particular traffic intensity,  $\nu = 5.0$ , and for  $N = 10, 30$ . Note that the  $N = 10$  curve overlies the  $N = 30$  curve. In general, as  $\lambda_J \rightarrow \lambda_J^{\{R_o, C\}}$ ,  $\eta^{\{R_o, C\}}$  increases to some finite maximum value at  $\lambda_J^{\{R_o, C\}}$ . Observe how  $\eta^{\{R_o, C\}}$  increases drastically as  $\lambda_J$  nears  $\lambda_J^{\{R_o, C\}}$ , and that when  $\lambda_J < \lambda_J^{\{R_o, C\}}$   $\eta^{\{R_o, C\}} = 1$ . Unity  $\eta^{\{R_o, C\}}$  occurs because, for the given value of  $\nu$ , when  $\hat{\lambda}_J^{\{R_o, C\}} < \lambda_J < \lambda_J^{\{R_o, C\}}$ , then  $\nu < \nu^{\{R_o, C\}}$  and CDMA is no longer the optimal protocol. be less than the noise limit for a given value of  $\nu$ , then  $\nu < \nu^{\{R_o, C\}}$  and CDMA is no longer the optimal protocol. Finally, note that by using Figs. 10-15, it is possible to estimate  $\eta^{\{R_o, C\}}$  for any values of  $\lambda_J$ ,  $\nu$ , and  $N$ , because of the nearly linear dependency of  $\eta^{\{R_o, C\}}$  on  $\nu$ .

Fig. 16-17 summarize the dependency of the optimal code rate  $\{R_o^*, C^*\}$  on the bit energy-to-jammer noise ratio  $\lambda_J$ , with and without jammer state information, respectively. Note that the selection of the optimal code rate depends primarily upon  $\nu$ ,  $\lambda_J$  and the availability of jammer state information, and does not depend on  $N$ . When  $\lambda_J = \infty$  and  $\nu < \nu^{\{R_o, C\}}$ , the optimal code rate  $\{R_o^*, C^*\}$  is unity. Hence, the optimal protocol is plain

ARQ. In fact, plain ARQ is used *only* when  $\lambda_J = \infty$  and  $\nu < \nu^{\{R_o, C\}}$ . When  $\lambda_J < \infty$  and  $\nu < \nu^{\{R_o, C\}}$ ,  $\{0.454, 0.500\} < \{R_o^*, C^*\} < 1.0$  when jammer state information is available, and  $\{0.247, 0.379\} < \{R_o^*, C^*\} < 1.0$  when it is not. In either case, Hybrid ARQ is used. For  $\lambda_J \leq \infty$  and  $\nu > \nu^{\{R_o, C\}}$ ,  $0.454 < R_o^* < 0.480$  and  $C^* = 0.500$  when jammer state information is available, and  $\{0.247, 0.379\} < \{R_o^*, C^*\} < \{0.480, 0.500\}$  when it is not. CDMA is the optimal protocol in this case. Note that for a given level of jammer noise, the optimal code rate can be determined as the traffic intensity varies by using Figs. 10-11 and 16-17. For a given  $\lambda_J$ , Figs. 10-11 gives the corresponding  $\nu^{\{R_o, C\}}$ . As the traffic intensity varies above and below this particular  $\nu^{\{R_o, C\}}$ , the optimal code rate is given by the lower branch and upper branch of Figs. 16-17, respectively.

The dependency of  $\rho^{\{R_o, C\}}$  on  $\lambda_J$  is shown in Figs. 18-19, with and without jammer state information, respectively. As with the code rate, the selection of the optimal jamming fraction depends primarily upon  $\nu$  and  $\lambda_J$ , and the availability of jammer state information. The optimal jamming fraction does not depend on the population size. Observe that if  $\nu < \nu^{\{R_o, C\}}$ , then  $\rho^{\{R_o, C\}} \rightarrow 0$  as  $\lambda_J \rightarrow \infty$ . If  $\nu > \nu^C$ , then  $\rho^C \rightarrow 1$  as  $\lambda_J \rightarrow \infty$  with or without jammer state information. If  $\nu > \nu^{R_o}$ , then  $\rho^{R_o} \rightarrow 1$  as  $\lambda_J \rightarrow \infty$  with jammer state information. However, without jammer state information,  $\rho^{R_o} \rightarrow 0$  as  $\lambda_J \rightarrow \infty$  with a scalloped appearance.

#### IV-A.3 Throughput-Delay Performance at Constant Jammer Power

Fig. 20 is a plot of the maximin normalized throughput  $T_{R_o}$  against traffic intensity for the case of constant jammer power. Fig. 21 is a plot of the corresponding maximin normalized throughput versus average packet delay  $D$ . Results are obtained for  $N = 10$  and  $\infty$ , with jammer state information, and for  $\tilde{\lambda}_J^{\{R_o, C\}}$  ranging from  $-10$  dB to  $\infty$  dB. Results for  $N = \infty$  provide a lower limit on performance. If  $\tilde{\lambda}_J < \hat{\lambda}_J^{\{R_o, C\}}$ , then a cutoff intensity does not exist and the throughput increases gradually with the traffic intensity. In this case, both both coding ( $r < 1.0$ ) and processing gain ( $\eta > 1.0$ ) are necessary to achieve a nonzero throughput. Recall that for the constant  $\lambda_J$  analysis, when  $\lambda_J < \hat{\lambda}_J^{\{R_o, C\}}$  then throughput was zero because  $\hat{\lambda}_J^{\{R_o, C\}}$  represented the smallest jammer noise level that can be present for



reliable coded communication in the absence of multiple-access interference. If  $\tilde{\lambda}_J \geq \hat{\lambda}_J^{\{R_o, C\}}$ , then a cutoff intensity exists and the throughput-traffic intensity characteristic is similar in form to that obtained in the constant  $\lambda_J$  analysis. For  $\tilde{\lambda}_J \geq \hat{\lambda}_J^{\{R_o, C\}}$  and  $\nu < \nu^{\{R_o, C\}}$ , coding alone is sufficient to overcome the effects of jamming ( $\eta = 1$ ).

Fig. 22 summarizes the dependency of  $\hat{m}$  on the traffic intensity  $\nu$  and the bit energy-to-jammer noise ratio  $\tilde{\lambda}_J$ , for a population size of  $N = 10$ . This diagram is very useful because it inherently summarizes the dependency of the optimal processing gain, code rate, and jamming fraction on  $\nu$  and  $\tilde{\lambda}_J$ . To see this, observe that for a given  $\tilde{\lambda}_J$ ,  $\hat{m}$  remains constant over a certain range of  $\nu$ . For each  $\{\tilde{\lambda}_J, \hat{m}\}$ , there is a corresponding  $\eta^{\{R_o, C\}}$ ,  $\{R_o^*, C^*\}$ , and  $\rho^{\{R_o, C\}}$  which also remain constant over that range of traffic intensity. Finally, for a given value of  $\hat{m}$ , the corresponding  $\eta^{\{R_o, C\}}$ ,  $\{R_o^*, C^*\}$ , and  $\rho^{\{R_o, C\}}$  do not depend on the population size. These results are shown in Figs. 23-25.

Results for the capacity case with jammer state information are shown in Figs. 26-31. Results for the cutoff rate and capacity cases without jammer state information closely follow the results for the case with jammer state information, and are not given here. Partial results for the cutoff rate case without jammer state information are reported in [24].

## V Operational Considerations

The results presented above suggest that the network will operate in one of three modes: plain ARQ, Hybrid ARQ, or CDMA. The mode of operation selected depends primarily upon the traffic intensity  $\nu$ , the level of jammer noise  $\lambda_J$ , and, to a lesser degree, upon the population size  $N$  and the availability of jammer state information. All of these quantities must be monitored by each transmitter for proper network operation. Two situations are possible depending upon the jammer noise level:  $\tilde{\lambda}_J > \hat{\lambda}_J$  which includes both the constant  $\lambda_J$  and constant jammer power cases, and  $\tilde{\lambda}_J < \hat{\lambda}_J$  which involves only the constant jammer power case.

First, consider the situation where  $\tilde{\lambda}_J > \hat{\lambda}_J$ . When the traffic intensity is low enough to permit stable network operation ( eg.,  $\nu < 0.5$  ), the network will operate in the plain ARQ mode when  $\tilde{\lambda}_J = \infty$  and in Hybrid ARQ mode when  $\tilde{\lambda}_J < \infty$ . In this

case, a transmitter will have to decide whether it wants to operate with optimal delay (upper  $p_r^*$  values in Fig. 9), with optimal throughput (lower  $p_r^*$  values in Fig. 9) by choosing the appropriate probability of retransmission, or with some non-optimal throughput-delay combination somewhere in between. While in either mode of operation, the probability of retransmission is adjusted according to variations in the traffic intensity and the population size (Fig. 9) and the code rate is adjusted to changes in the jammer noise level depending upon the availability of jammer state information (Figs. 16-17). When the traffic intensity reaches a certain level ( $0.5 \leq \nu \leq 1.0$ ), the network becomes unstable. As the traffic intensity continues to increase, a cutoff intensity is eventually reached where the optimal protocol becomes CDMA. In order to determine when to switch to CDMA, the traffic intensity could be monitored. In the case of finite population systems, the number of backlogged transmitters or the traffic intensity could be monitored. While in the CDMA mode of operation, the probability of retransmission is adjusted according to variations in the traffic intensity and population size (Fig. 9), and the processing gain is adjusted according to changes in the traffic intensity, the jammer noise level, and the population size (Figs. 10-15). The code rate is adjusted to changes in the jammer noise level depending upon the availability of jammer state information (Figs. 16-17). Note that with jammer state information, the code rate remains virtually constant.

For the situation where  $\tilde{\lambda}_J < \hat{\lambda}_J$ , the CDMA protocol is employed exclusively. Optimal values of  $p_r$  are selected according to variations in the traffic intensity and population size (Fig. 9). The processing gain and code rate are adjusted according to changes in  $\nu$  and  $\lambda_J$  (Figs. 20-31).

## VI Concluding Remarks

In this paper, we have examined the throughput-delay performance of Type I hybrid ARQ protocols in a slotted direct-sequence CDMA paired-off network operating in a hostile jamming environment. Numerical analyses were presented to show how network design parameters such as the retransmission probability, code rate, and processing gain should be chosen in order to maximize system performance. The effects of pulse jamming, with and

without jammer state information, were also examined. Important descriptive parameters such as the cutoff traffic intensity, jammer noise limits, and asymptotic jammer noise limits helped illustrate when it is best to use one of the error control methods discussed in this paper (ARQ, hybrid ARQ, CDMA).

## References

- [1] M. Pursley, "The Role of Spread Spectrum in Packet Radio Networks," *Proceedings of the IEEE*, vol. 75, pp. 116-134, Jan. 1987.
- [2] J. M. K. Simon, *Spread Spectrum Communications*. Computer Science Press, 1985.
- [3] D. Raychaudhuri, "Performance Analysis of Random Access Packet-Switched Code Division Multiple Access Systems," *IEEE Transactions on Communications*, vol. COM-29, pp. 895-901, June 1981.
- [4] J. Hui, "Throughput Analysis for Code Division Multiple Access of the Spread Spectrum Channel," *IEEE Journal on Selected Areas in Communications*, vol. 2, pp. 482-486, July 1984.
- [5] A. Polydoros and J. Silvester, "Slotted Random Access Spread-Spectrum Networks: An Analytical Framework," *IEEE Journal on Selected Areas in Communications*, vol. SAC-5, pp. 989-1001, July 1987.
- [6] G. L. Stuber, "Asymptotic Throughput in Slotted Direct-Sequence Code Division Multiple-Access Networks," in *Proc. MILCOM'88*, pp. 44.6.1-44.6.5, October 1988.
- [7] J. M. Hanratty and G. L. Stuber, "Asymptotic Performance Analysis of Hybrid ARQ Protocols in Slotted Direct-Sequence Code Division Multiple-Access Networks," in *Proc. INFOCOM'89*, vol. II, pp. 574-583, Apr. 1989.
- [8] N. B. Pronios and A. Polydoros, "Slotted ALOHA-type Fully Connected Networks in Jamming Part I: Unspread ALOHA," in *Proc. MILCOM'87*, vol. 3, pp. 44.1.1-44.1.5, 1987.
- [9] S. Lin and D. J. Costello, Jr., *Error Control Coding: Fundamentals and Applications*. New Jersey: Prentice-Hall, 1983.
- [10] R. J. McEliece and W. E. Stark, "Channels with Block Interference," *IEEE Transactions on Information Theory*, vol. IT-30, pp. 44-53, Jan. 1984.
- [11] M. B. Pursley, "Performance Evaluation for Phase-Coded Spread Spectrum Multiple-Access Communication - Part I: System Analysis," *IEEE Transactions on Communications*, vol. 25, pp. 793-799, Aug. 1977.
- [12] E. Geraniotis and M. Pursley, "Error Probabilities for Direct-Sequence Spread-Spectrum Multiple-Access Communications - Part II," *IEEE Transactions on Communications*, vol. 30, pp. 985-995, May 1982.
- [13] J. Lehnert and M. Pursley, "Error Probabilities for Binary Direct-Sequence Spread-Spectrum Communications with Random Signature Sequences," *IEEE Transactions on Communications*, vol. 35, pp. 87-98, Jan. 1987.
- [14] E. Geraniotis, "Performance of Noncoherent Direct Sequence Spread-Spectrum Multiple-Access Communications," *IEEE Journal on Selected Areas in Communications*, vol. 3, pp. 687-694, Sep. 1985.

- [15] C. L. Weber and et. al., "Performance Considerations of Code Division Multiple-Access Systems," *IEEE Transactions on Vehicular Technology*, vol. VT-30, pp. 3-9, February 1981.
- [16] J. Massey, "Coding and Modulation in Digital Communications," *Proc. Int. Zurich Sem. Digital Commun.*, pp. E2(1)-E2(4), 1974.
- [17] F. Jelinek, "A Fast Sequential Decoding Algorithm Using a Stack," *IBM Journal. Res. Dev.*, vol. 13, pp. 675-685, Nov. 1969.
- [18] G. C. Clark and J. B. Cain, *Coding for Error Control*. New Jersey: Plenum Press, 1981.
- [19] G. L. Stuber, "Throughput Analysis of a Slotted Direct-Sequence Spread Spectrum Multiple-Access Network," *submitted to IEEE Transactions on Communications*, 1989.
- [20] S. El-Khamy and A. Balameshi, "Selection of Gold and Kasami Code Sets for Spread Spectrum CDMA Systems of Limited Number of Users," *Int. J. Satellite Commun.*, vol. 5, pp. 23-32, Jan-Mar 1987.
- [21] L. Klienrock, *Queueing Systems*. New York: John Wiley & Sons, Inc., 1975.
- [22] S. S. Lam, *Packet Switching in a Multi-access Broadcast Channel with Application to Satellite Communication in a Computer Network*. PhD thesis, Dep. Comput. Sci., Univ. Calif., Los Angeles, 1974.
- [23] J. M. Hanratty, *Performance Analysis of Hybrid ARQ Protocols in a Slotted Code Division Multiple-Access Network*. PhD thesis, Sch of Electrical Engineering, Georgia Institute of Technology, Atlanta Georgia, 1989.
- [24] J. M. Hanratty and G. L. Stuber, "Performance Analysis of Hybrid ARQ Protocols in Slotted Direct-Sequence Code Division Multiple-Access Networks: Jamming Analysis," *to appear in MILCOM'89*, 1989.

## List of Illustrations

- Figure 1 CDMA Network Packet Flow Model
- Figure 2 Type I Hybrid ARQ System
- Figure 3 Maximin Normalized Throughput ( $T_{\{R_o, C\}}$ ) versus Traffic Intensity ( $\nu$ )  
for  $N = 10$
- Figure 4 Maximin Normalized Throughput ( $T_{\{R_o, C\}}$ ) versus Traffic Intensity ( $\nu$ )  
for  $N = 30$
- Figure 5 Average Packet Delay ( $D$ ) versus Maximin Normalized Throughput ( $T_{\{R_o, C\}}$ )  
for  $N = 10$  (Jammer State Information)
- Figure 6 Average Packet Delay ( $D$ ) versus Maximin Normalized Throughput ( $T_{\{R_o, C\}}$ )  
for  $N = 10$  (No Jammer State Information)
- Figure 7 Average Packet Delay ( $D$ ) versus Maximin Normalized Throughput ( $T_{\{R_o, C\}}$ )  
for  $N = 30$  (Jammer State Information)
- Figure 8 Average Packet Delay ( $D$ ) versus Maximin Normalized Throughput ( $T_{\{R_o, C\}}$ )  
for  $N = 30$  (No Jammer State Information)
- Figure 9 Optimal Probability of Retransmission ( $p_r^*$ ) versus Traffic Intensity ( $\nu$ )
- Figure 10 Cutoff Traffic Intensity ( $\nu^{\{R_o, C\}}$ ) versus Bit Energy-to-Jammer Noise Ratio  
( $\lambda_J$ ) (Jammer State Information)
- Figure 11 Cutoff Traffic Intensity ( $\nu^{\{R_o, C\}}$ ) versus Bit Energy-to-Jammer Noise Ratio  
( $\lambda_J$ ) (No Jammer State Information)
- Figure 12 Optimal Processing Gain ( $\eta^{\{R_o, C\}}$ ) versus Traffic Intensity ( $\nu$ )  
for the Cutoff Rate Case
- Figure 13 Optimal Processing Gain ( $\eta^{\{R_o, C\}}$ ) versus Traffic Intensity ( $\nu$ )  
for the Capacity Case
- Figure 14 Optimal Processing Gain ( $\eta^{\{R_o, C\}}$ ) versus Bit Energy-to-Jammer Noise Ratio  
( $\lambda_J$ ) (Jammer State Information,  $\nu = 5.0$ )
- Figure 15 Optimal Processing Gain ( $\eta^{\{R_o, C\}}$ ) versus Bit Energy-to-Jammer Noise Ratio  
( $\lambda_J$ ) (No Jammer State Information,  $\nu = 5.0$ )
- Figure 16 Optimal Code Rate ( $R_o^*, C^*$ ) versus Bit Energy-to-Jammer Noise Ratio  
( $\lambda_J$ ) (Jammer State Information)
- Figure 17 Optimal Code Rate ( $R_o^*, C^*$ ) versus Bit Energy-to-Jammer Noise Ratio  
( $\lambda_J$ ) (No Jammer State Information)
- Figure 18 Optimal Jamming Fraction ( $\rho^{\{R_o, C\}}$ ) versus Bit Energy-to-Jammer Noise Ratio  
( $\lambda_J$ ) (Jammer State Information)
- Figure 19 Optimal Jamming Fraction ( $\rho^{\{R_o, C\}}$ ) versus Bit Energy-to-Jammer Noise Ratio  
( $\lambda_J$ ) (No Jammer State Information)
- Figure 20 Maximin Normalized Throughput ( $T_{\{R_o, C\}}$ ) versus Traffic Intensity ( $\nu$ )  
(Constant Jammer Power, Cutoff Rate Case, Jammer State Information)
- Figure 21 Average Packet Delay ( $D$ ) versus Maximin Normalized Throughput ( $T_{\{R_o, C\}}$ )  
(Constant Jammer Power, Cutoff Rate Case, Jammer State Information)
- Figure 22 Number of Simultaneous Users ( $\hat{n}$ ) versus Traffic Intensity ( $\nu$ ) versus  
Bit Energy-to-Jammer Noise Ratio ( $\tilde{\lambda}_J$ ) for  $N = 10$   
(Constant Jammer Power, Cutoff Rate Case, Jammer State Information)

- Figure 23** Optimal Processing Gain ( $\eta^{R_o}$ ) versus Traffic Intensity ( $\nu$ ) versus  
 Bit Energy-to-Jammer Noise Ratio ( $\tilde{\lambda}_J$ ) for  $N = 10$   
 (Constant Jammer Power, Cutoff Rate Case, Jammer State Information)
- Figure 24** Optimal Code Rate ( $R_o^*$ ) versus Traffic Intensity ( $\nu$ ) versus  
 Bit Energy-to-Jammer Noise Ratio ( $\tilde{\lambda}_J$ ) for  $N = 10$   
 (Constant Jammer Power, Cutoff Rate Case, Jammer State Information)
- Figure 25** Optimal Jamming Fraction ( $\rho^{R_o}$ ) versus Traffic Intensity ( $\nu$ ) versus  
 Bit Energy-to-Jammer Noise Ratio ( $\tilde{\lambda}_J$ ) for  $N = 10$   
 (Constant Jammer Power, Cutoff Rate Case, Jammer State Information)
- Figure 26** Maximin Normalized Throughput ( $T_{\{R_o, C\}}$ ) versus Traffic Intensity ( $\nu$ )  
 (Constant Jammer Power, Capacity Case, Jammer State Information)
- Figure 27** Average Packet Delay ( $D$ ) versus Maximin Normalized Throughput ( $T_{\{R_o, C\}}$ )  
 (Constant Jammer Power, Capacity Case, Jammer State Information)
- Figure 28** Number of Simultaneous Users ( $\hat{m}$ ) versus Traffic Intensity ( $\nu$ ) versus  
 Bit Energy-to-Jammer Noise Ratio ( $\tilde{\lambda}_J$ ) for  $N = 10$   
 (Constant Jammer Power, Capacity Case, Jammer State Information)
- Figure 29** Optimal Processing Gain ( $\eta^C$ ) versus Traffic Intensity ( $\nu$ ) versus  
 Bit Energy-to-Jammer Noise Ratio ( $\tilde{\lambda}_J$ ) for  $N = 10$   
 (Constant Jammer Power, Capacity Case, Jammer State Information)
- Figure 30** Optimal Code Rate ( $C^*$ ) versus Traffic Intensity ( $\nu$ ) versus  
 Bit Energy-to-Jammer Noise Ratio ( $\tilde{\lambda}_J$ ) for  $N = 10$   
 (Constant Jammer Power, Capacity Case, Jammer State Information)
- Figure 31** Optimal Jamming Fraction ( $\rho^C$ ) versus Traffic Intensity ( $\nu$ ) versus  
 Bit Energy-to-Jammer Noise Ratio ( $\tilde{\lambda}_J$ ) for  $N = 10$   
 (Constant Jammer Power, Capacity Case, Jammer State Information)

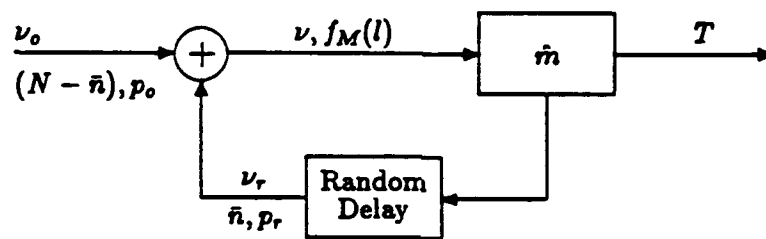


**Figure 1** CDMA Network Packet Flow Model



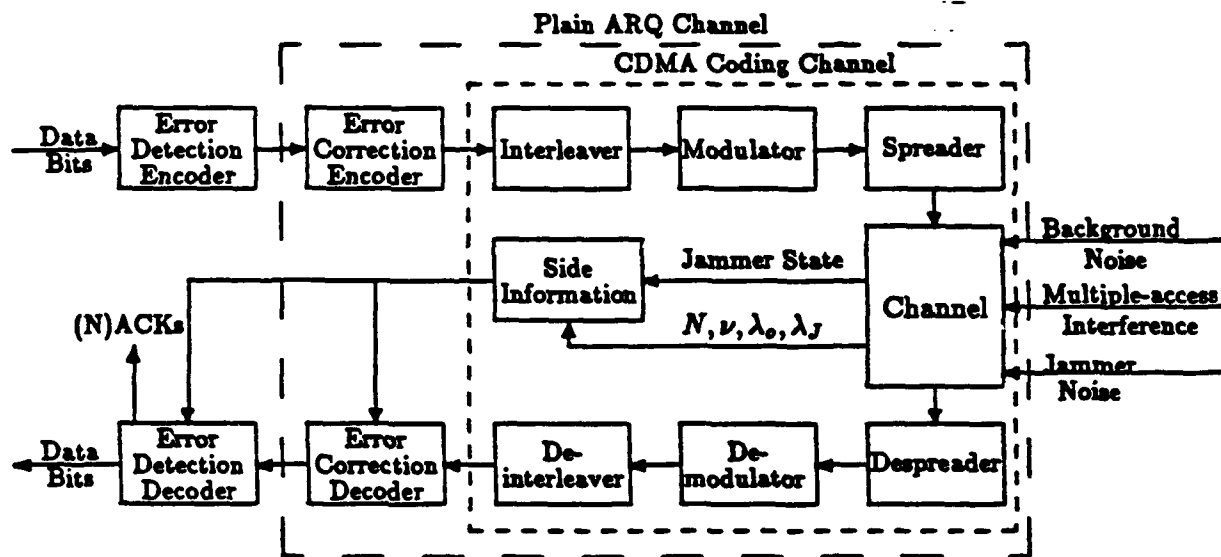


Figure 2: Type I Hybrid ARQ System

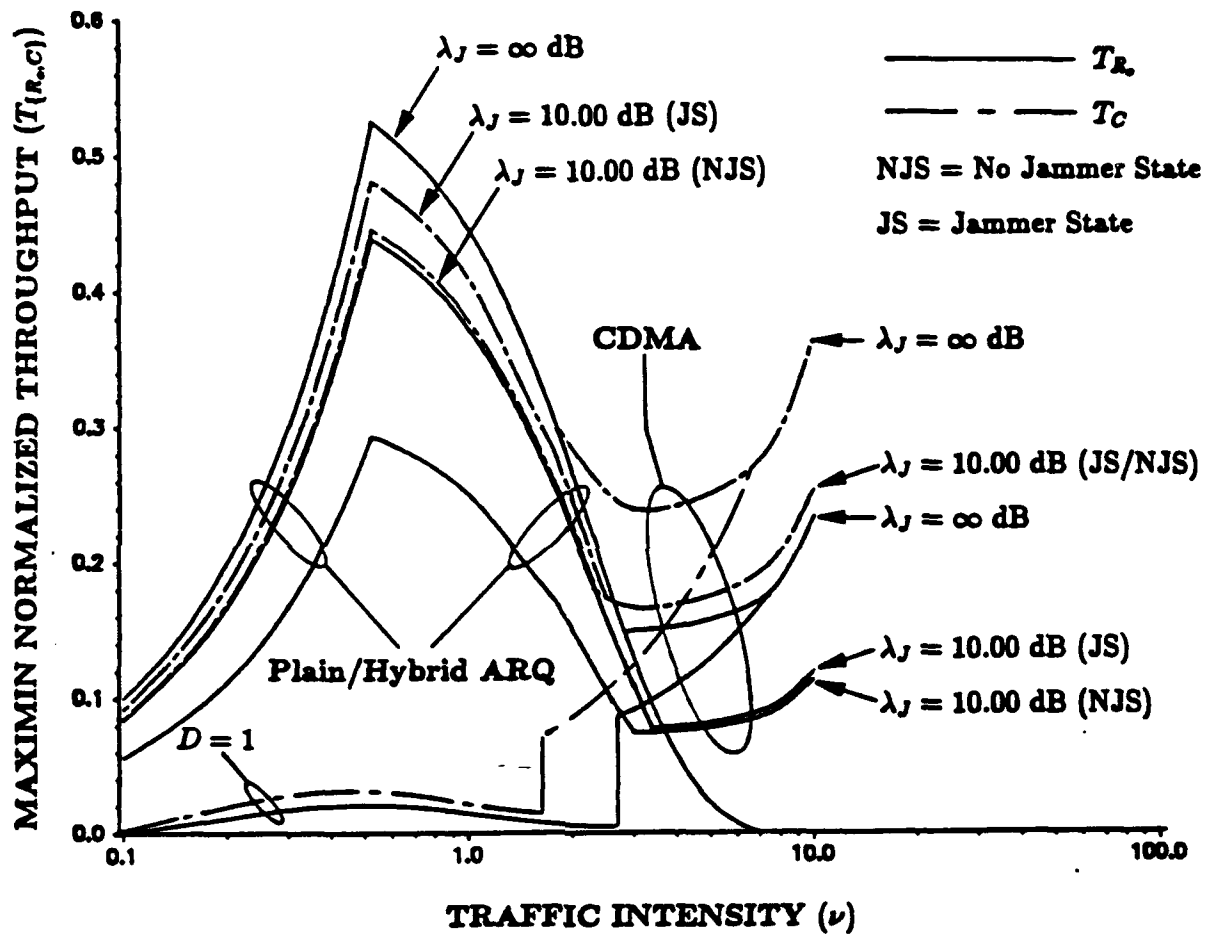


Figure 3: Maximin Normalized Throughput versus Traffic Intensity for  $N = 10$

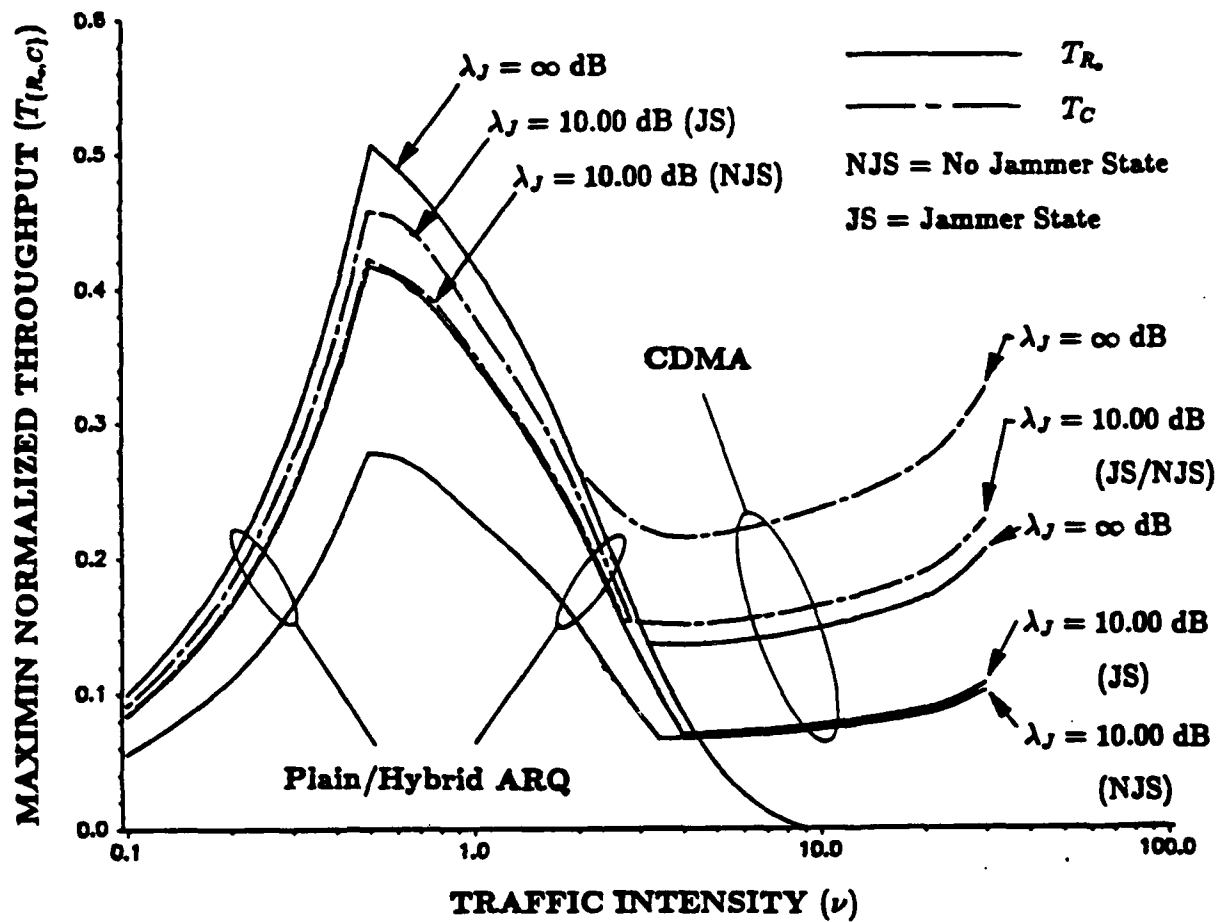


Figure 4: Maximin Normalized Throughput versus Traffic Intensity for  $N = 30$

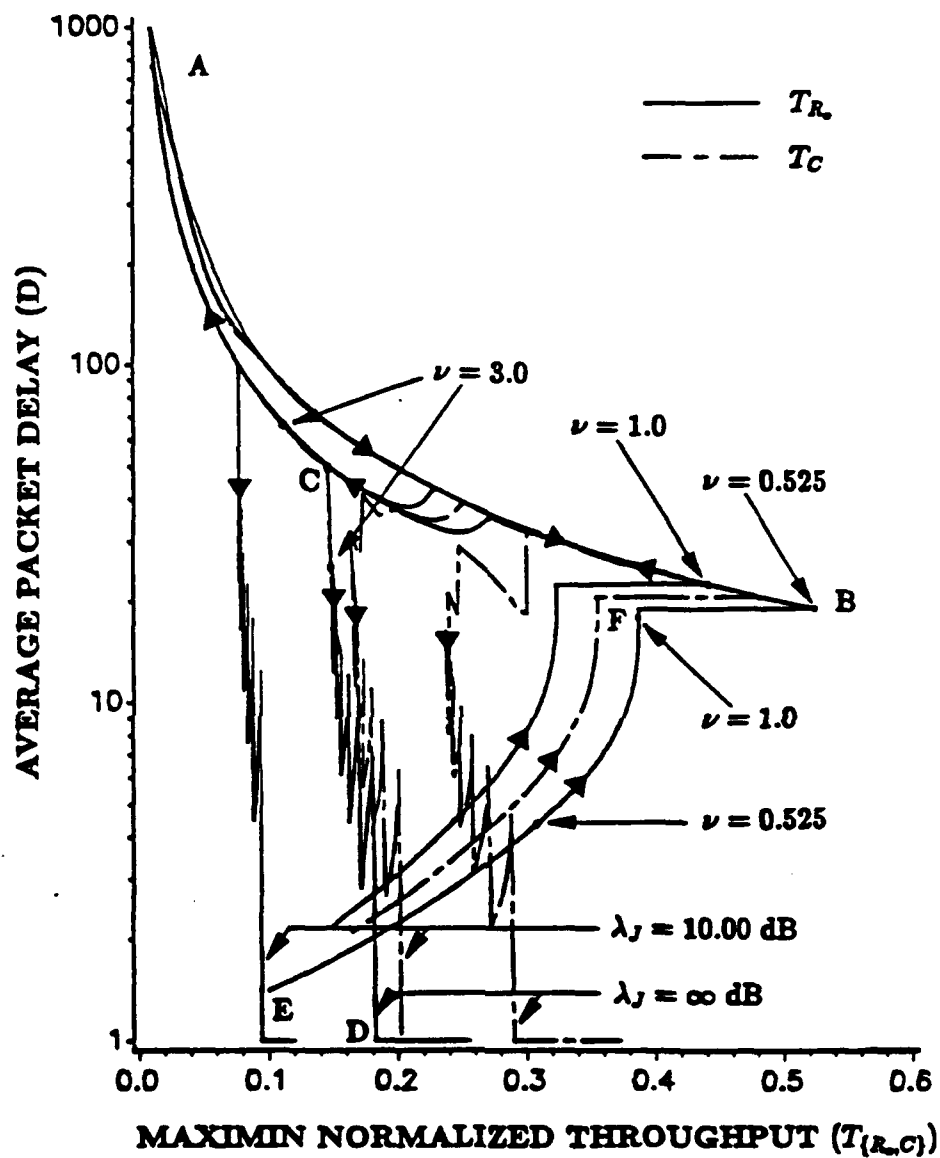


Figure 5: Average Packet Delay versus Maximin Normalized Throughput for  $N = 10$   
(Jammer State Information)

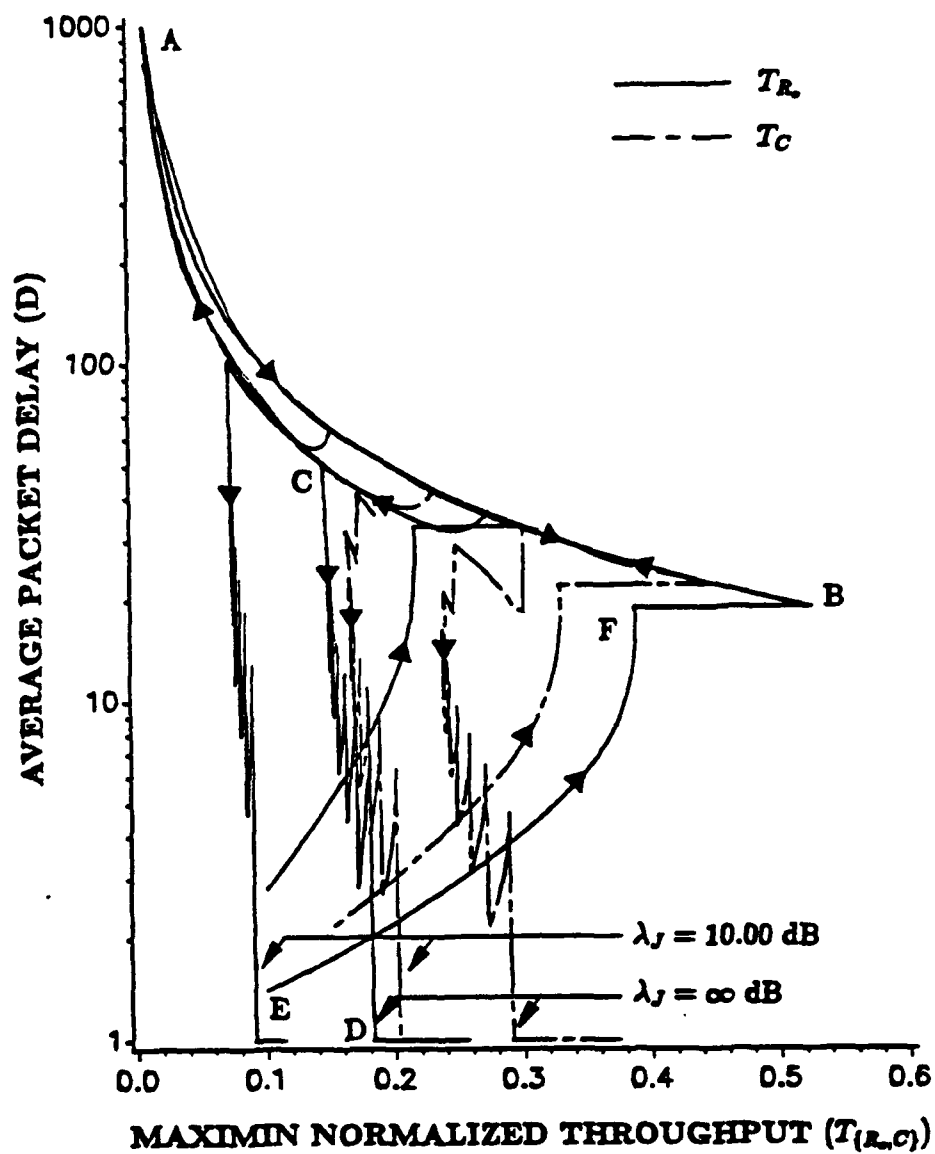


Figure 6: Average Packet Delay versus Maximin Normalized Throughput for  $N = 10$   
(No Jammer State Information)

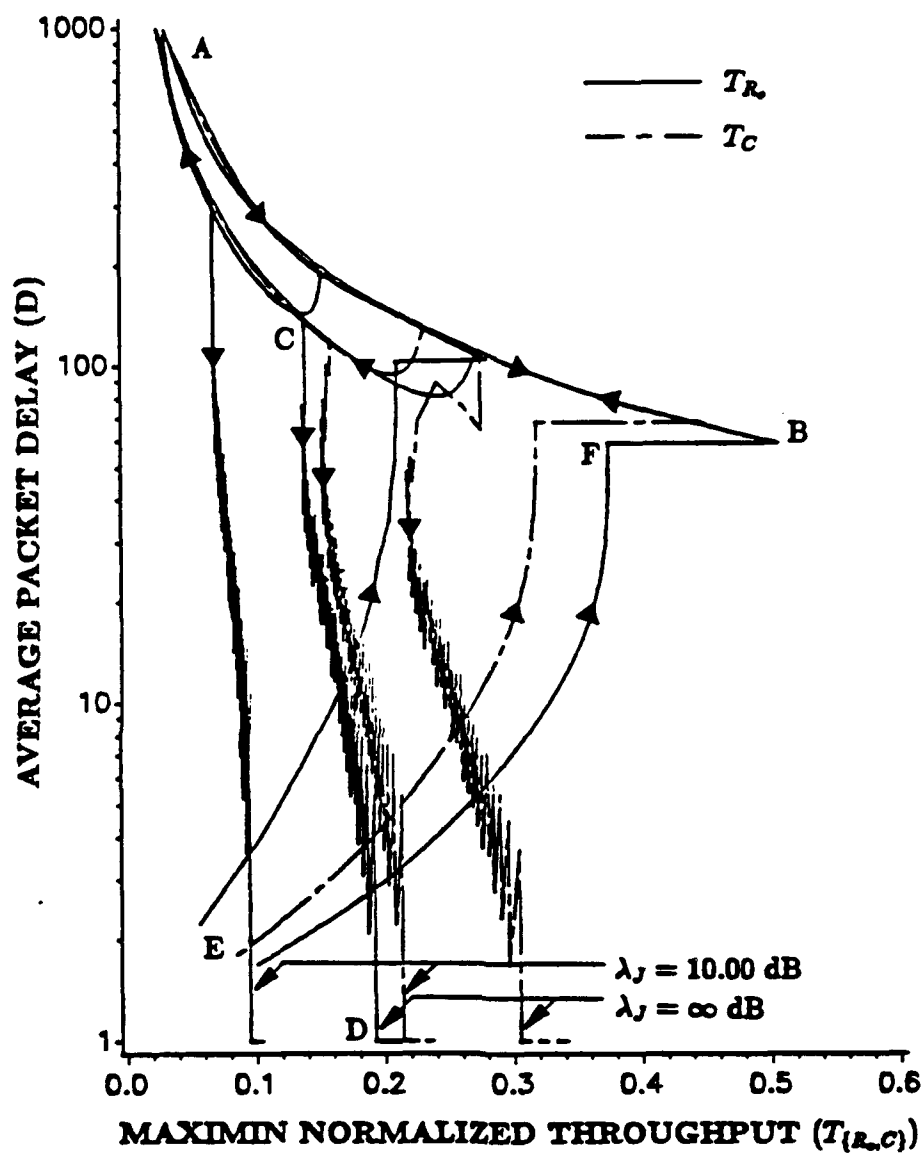


Figure 7: Average Packet Delay versus Maximin Normalized Throughput for  $N = 30$   
(Jammer State Information)

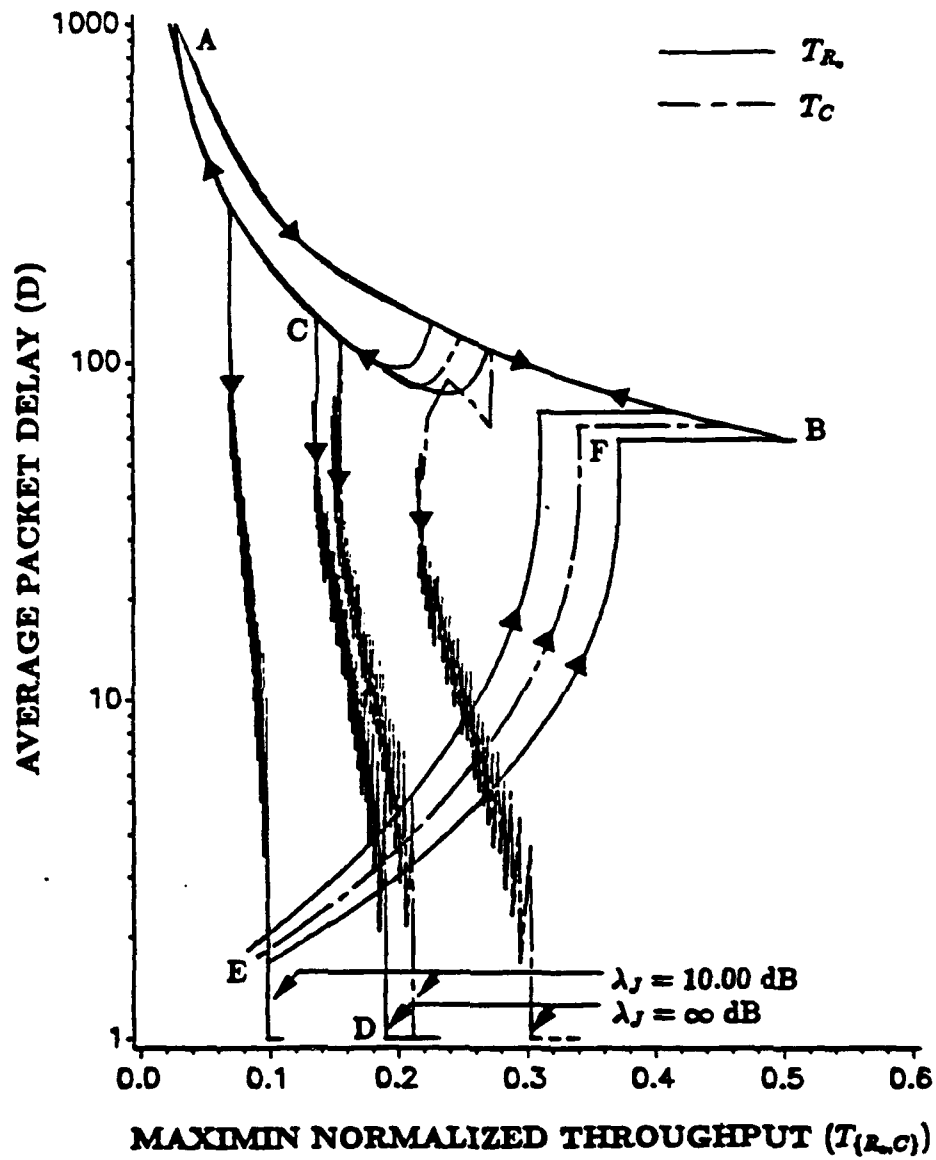


Figure 8: Average Packet Delay versus Maximin Normalized Throughput for  $N = 30$   
(No Jammer State Information)

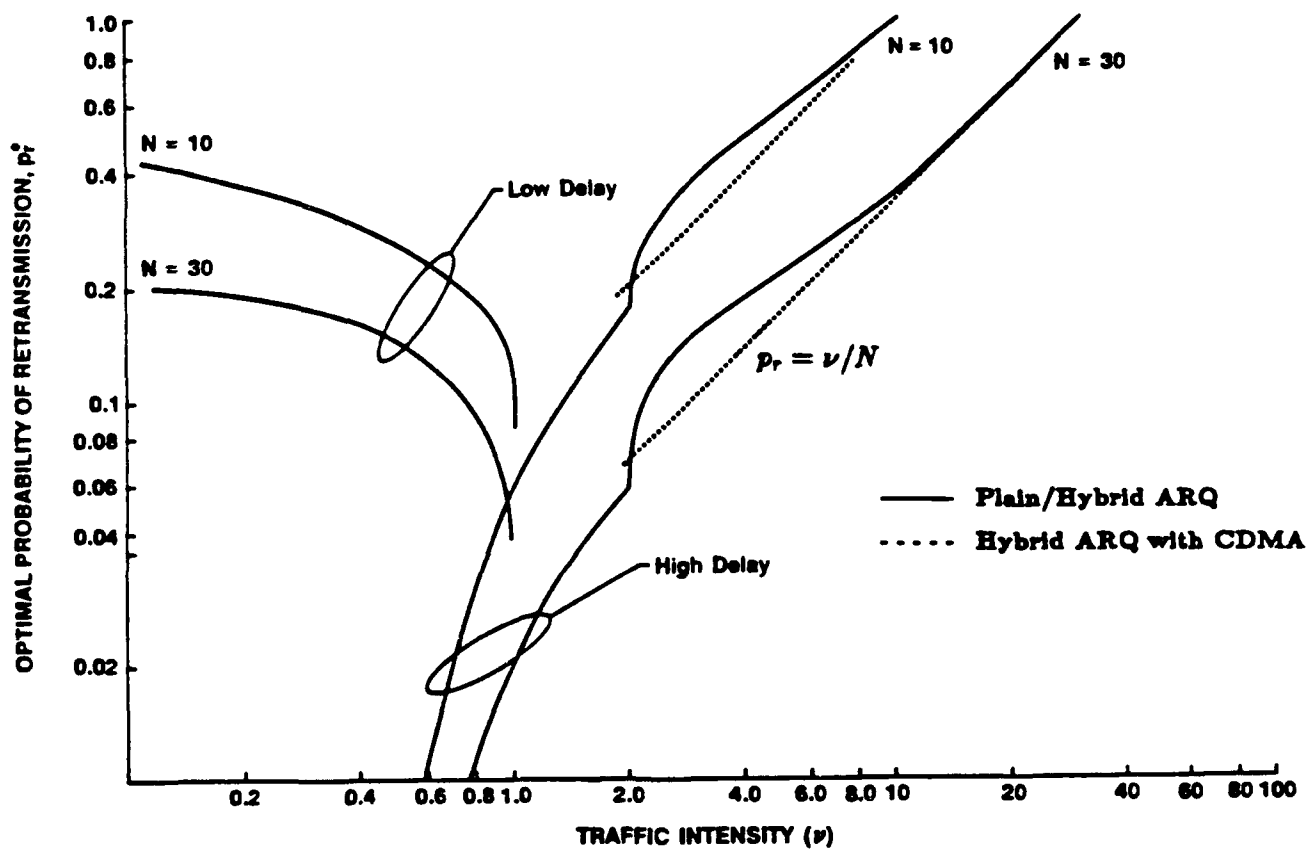


Figure 9: Optimal Probability of Retransmission ( $p_r^*$ ) versus Traffic Intensity ( $\nu$ ) for  $N = 10, 30$



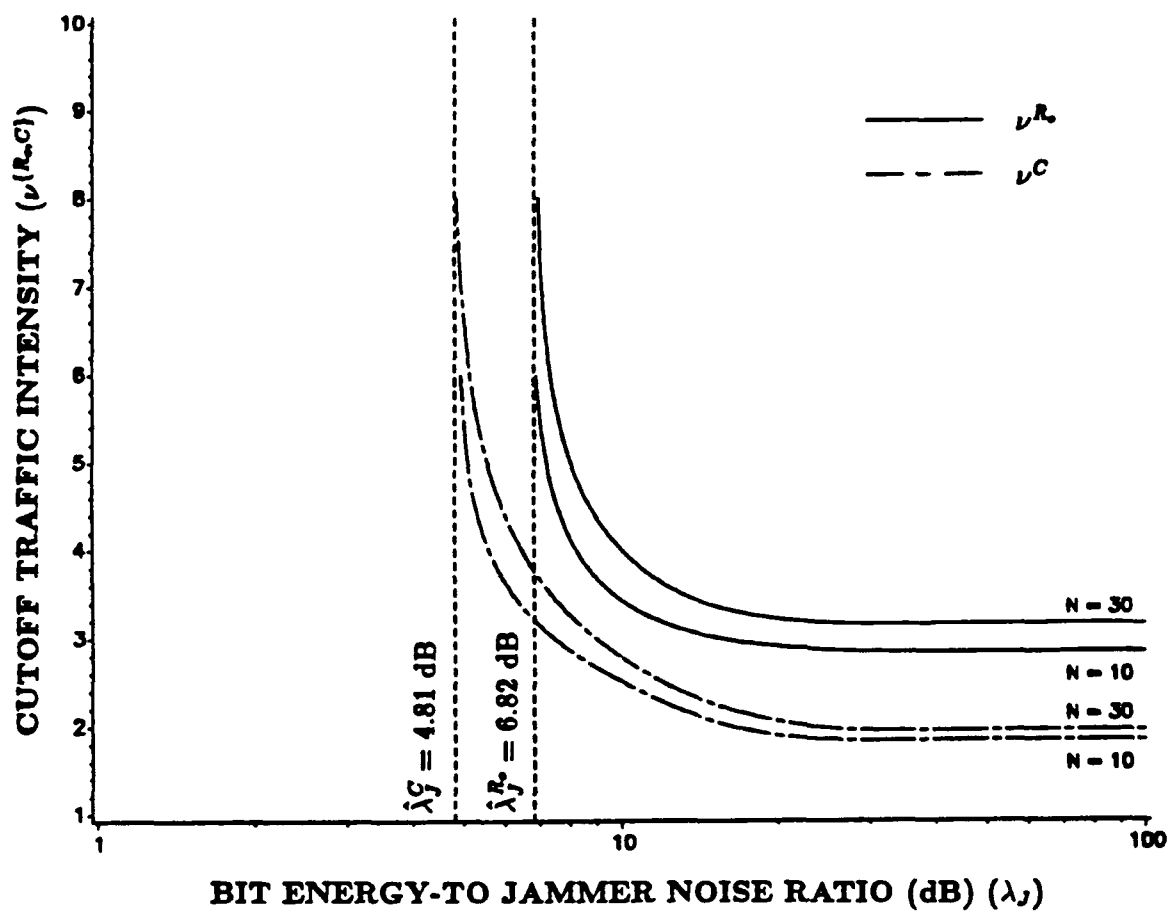


Figure 10: Cutoff Traffic Intensity versus Bit Energy-to-Jammer Noise Ratio  
(Jammer State Information)

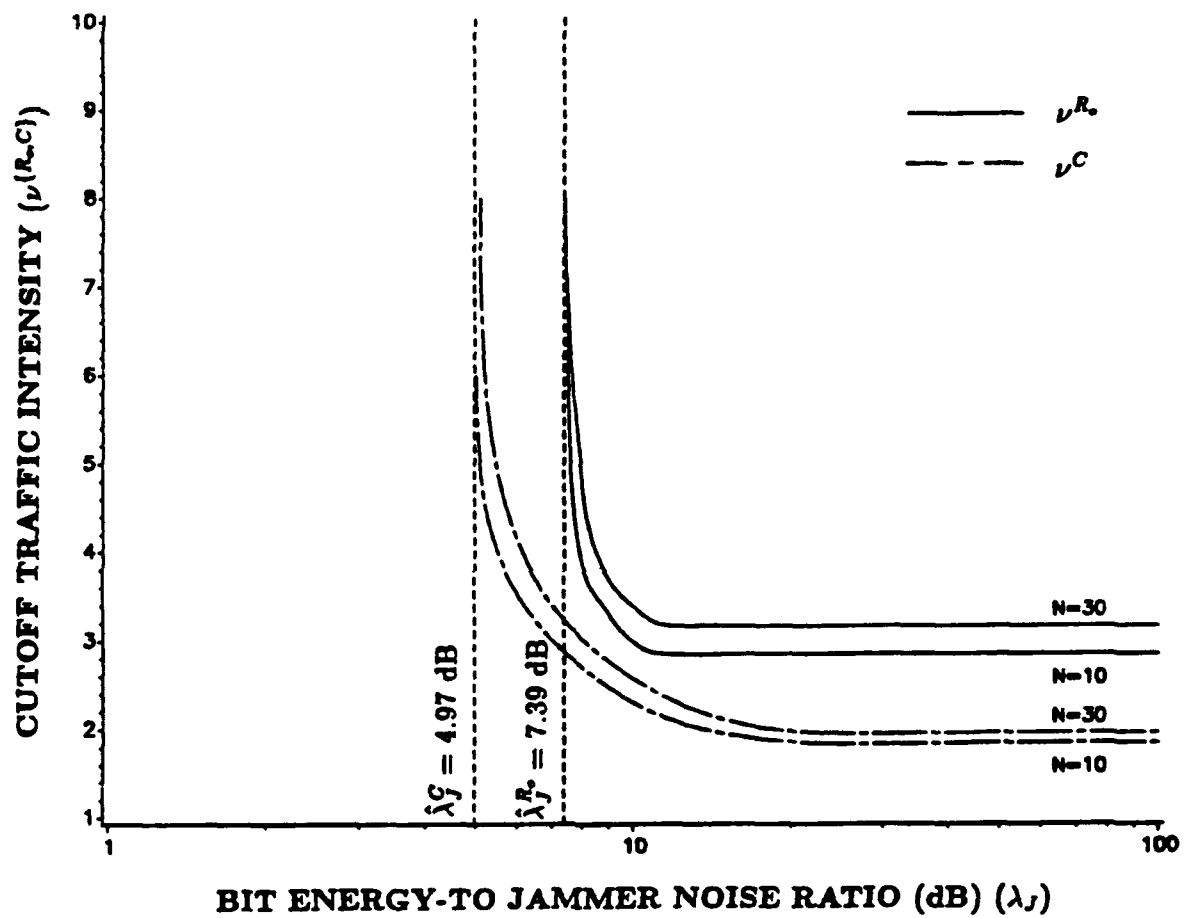


Figure 11: Cutoff Traffic Intensity versus Bit Energy-to-Jammer Noise Ratio  
(No Jammer State Information)

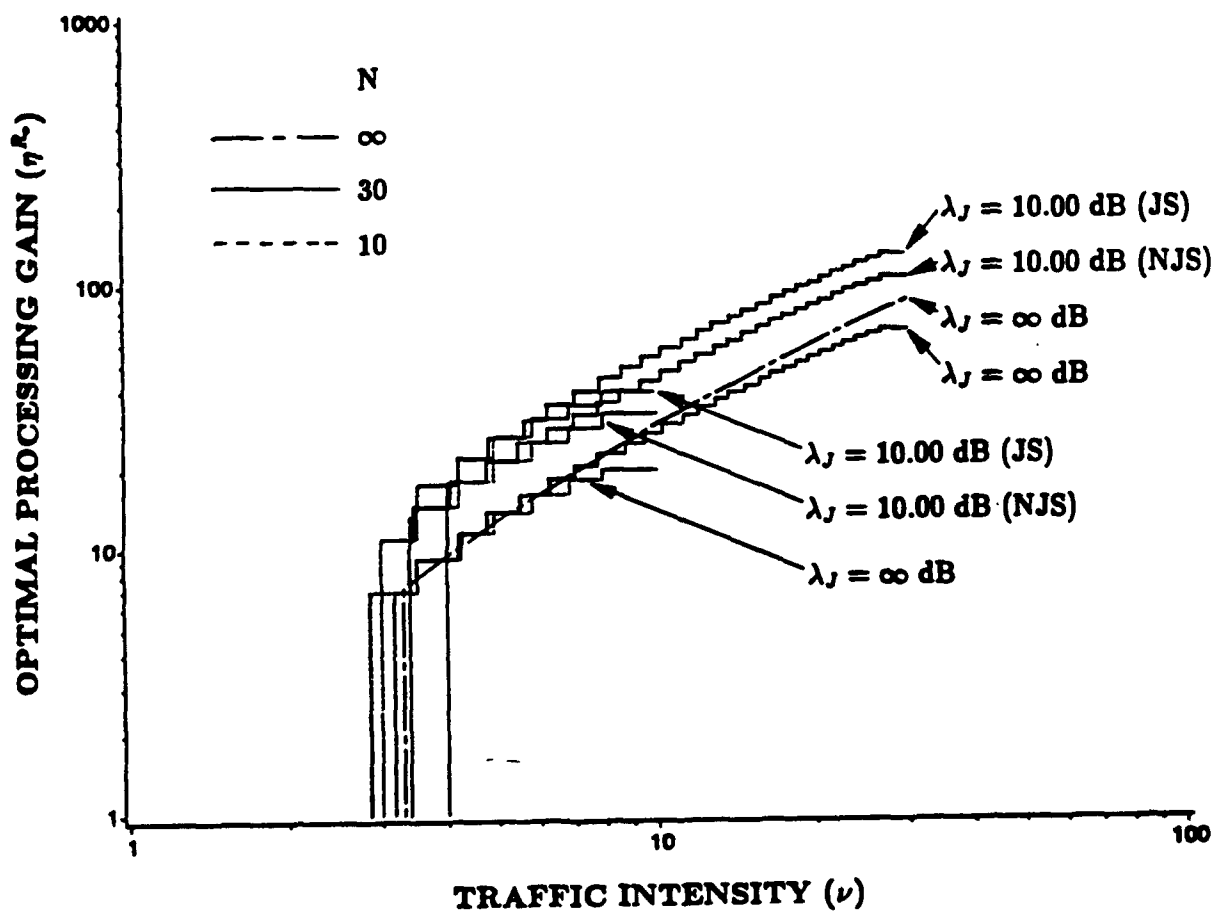


Figure 12: Optimal Processing Gain versus Traffic Intensity for the Cutoff Rate Case

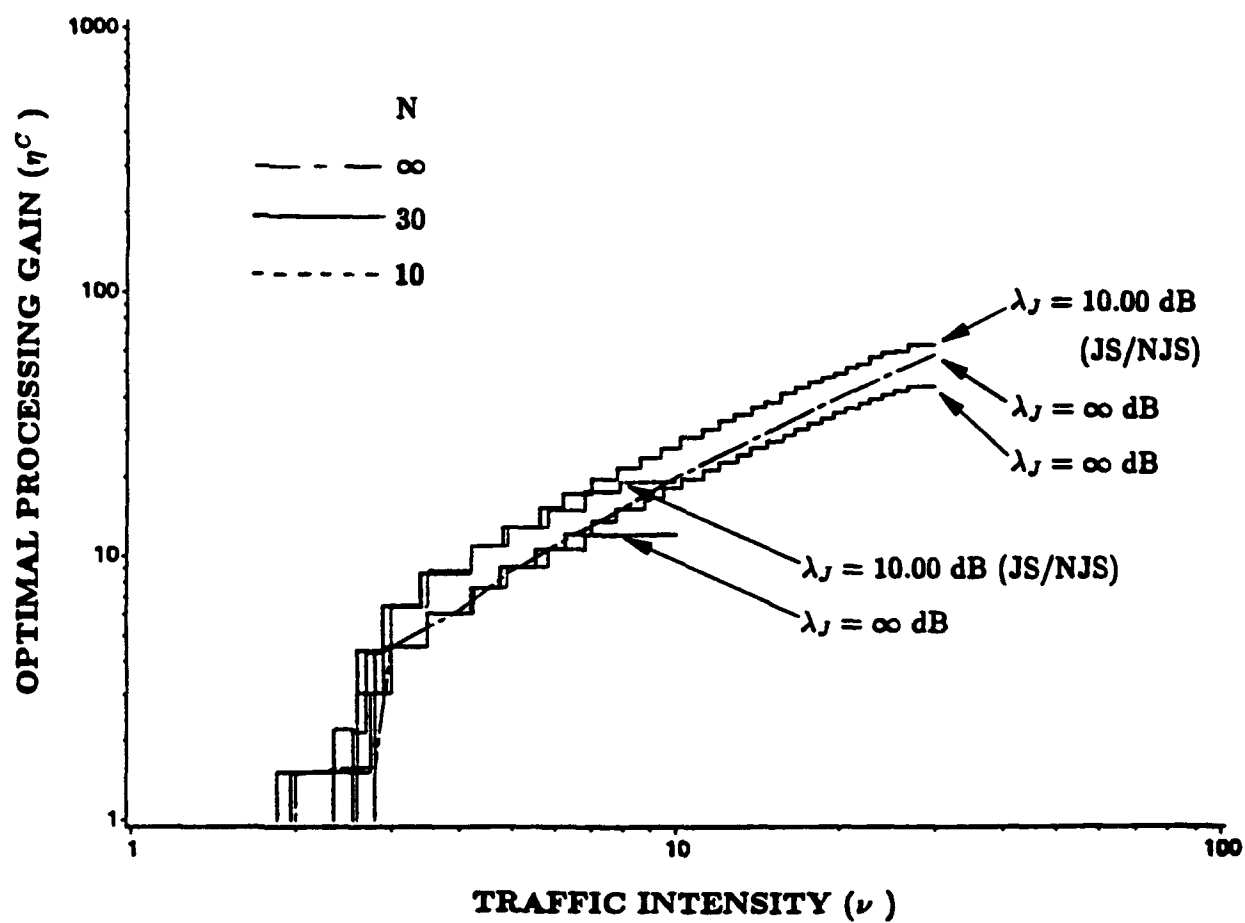


Figure 13: Optimal Processing Gain versus Traffic Intensity for the Capacity Case

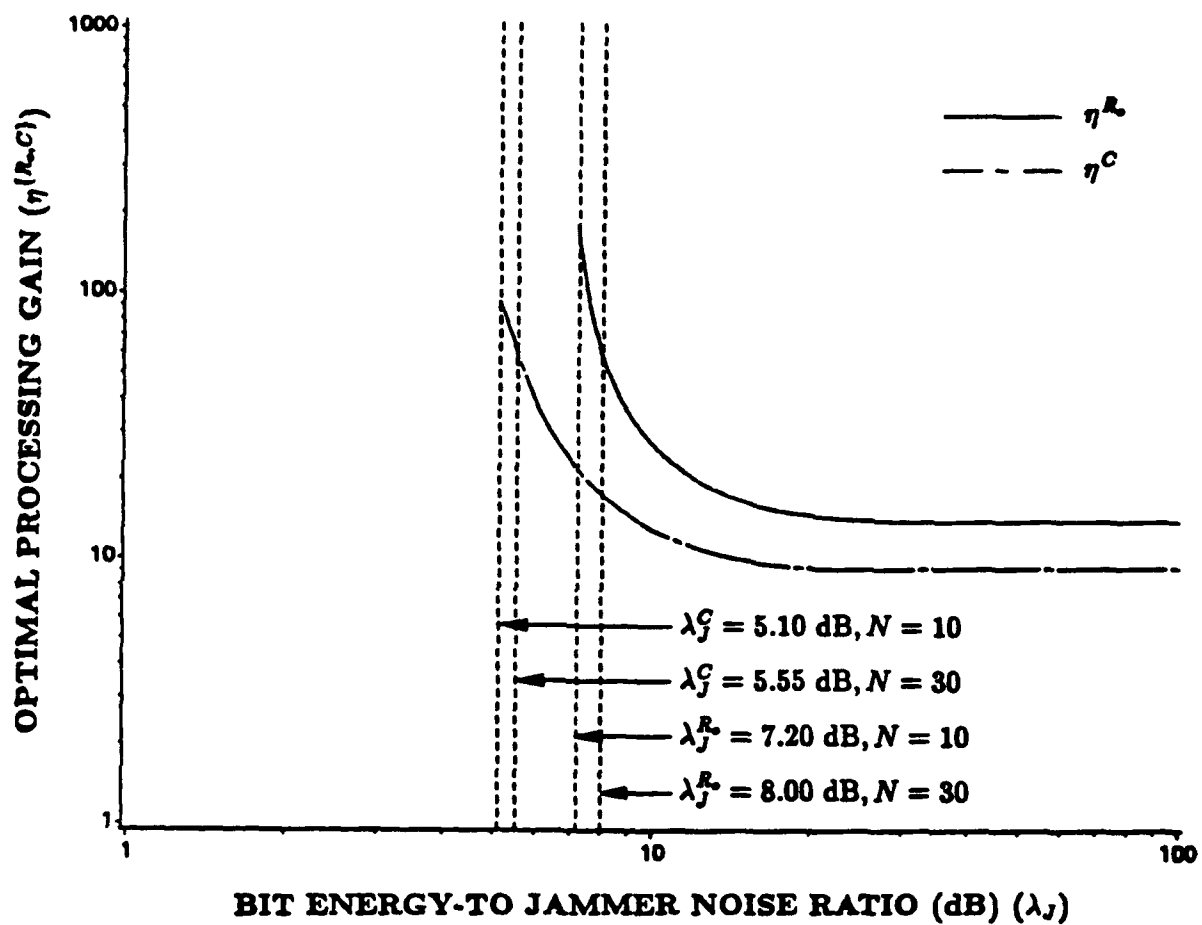


Figure 14: Optimal Processing Gain versus Bit Energy-to-Jammer Noise Ratio  
(Jammer State Information) ( $\nu = 5.0$ )

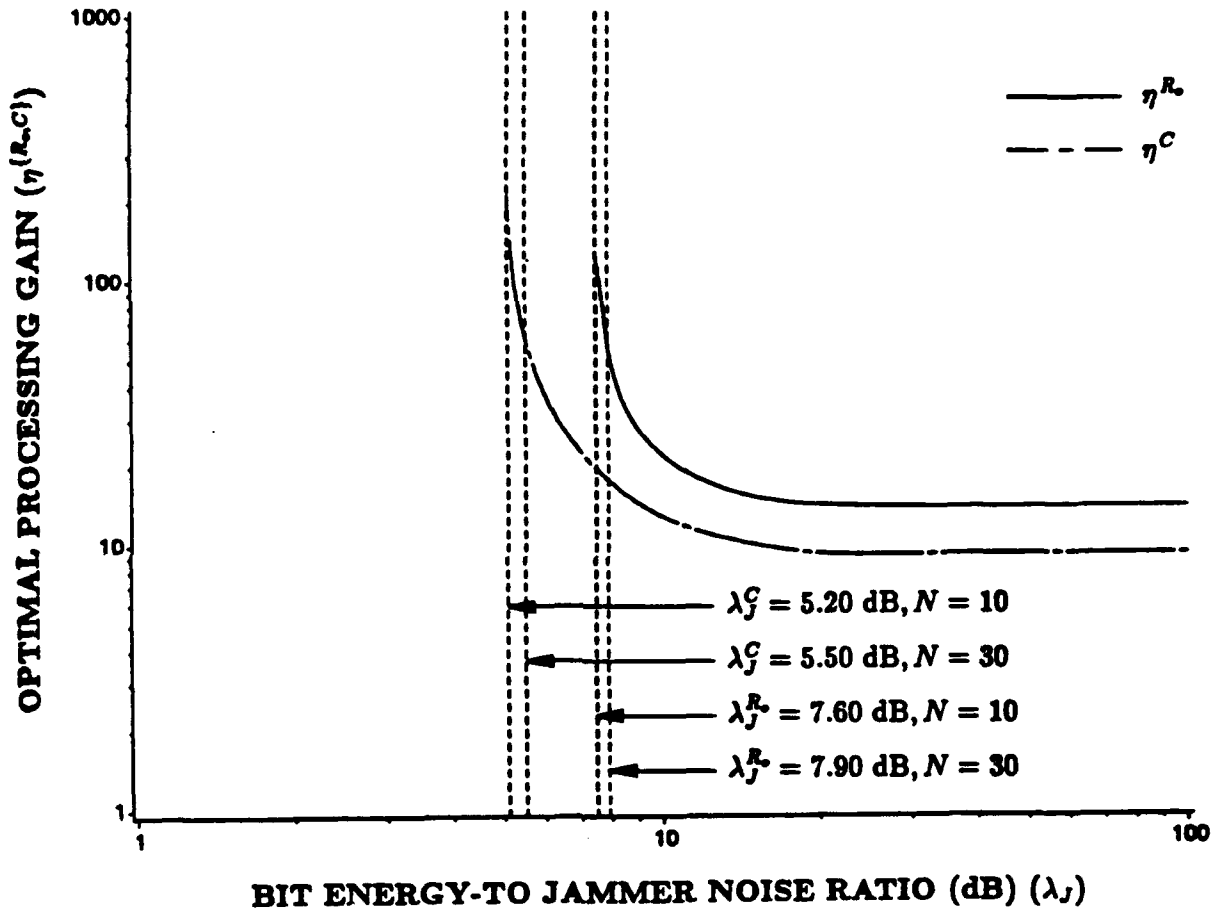


Figure 15: Optimal Processing Gain versus Bit Energy-to-Jammer Noise Ratio  
(No Jammer State Information) ( $\nu = 5.0$ )

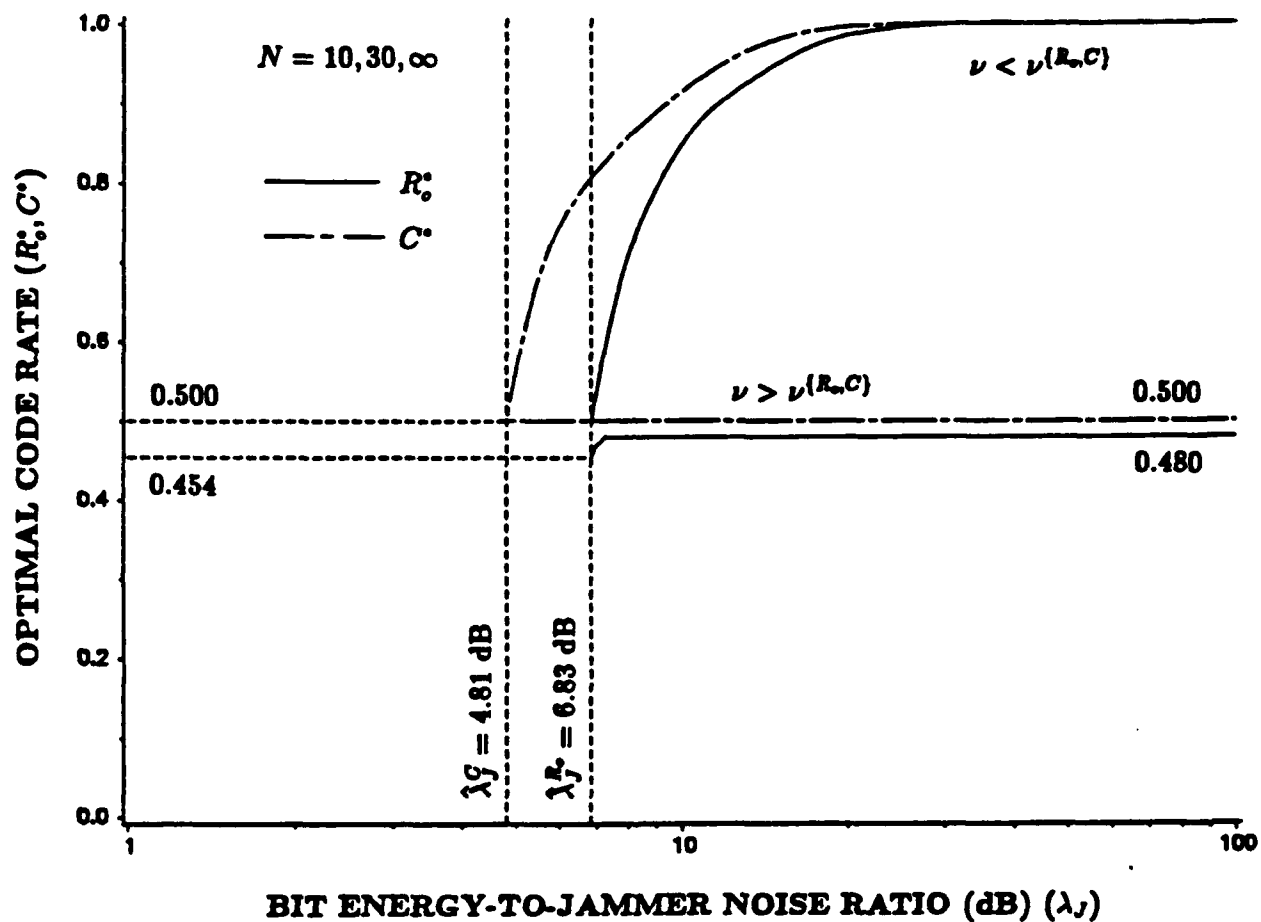


Figure 16: Optimal Code Rate versus Bit Energy-to-Jammer Noise Ratio  
(Jammer State Information)

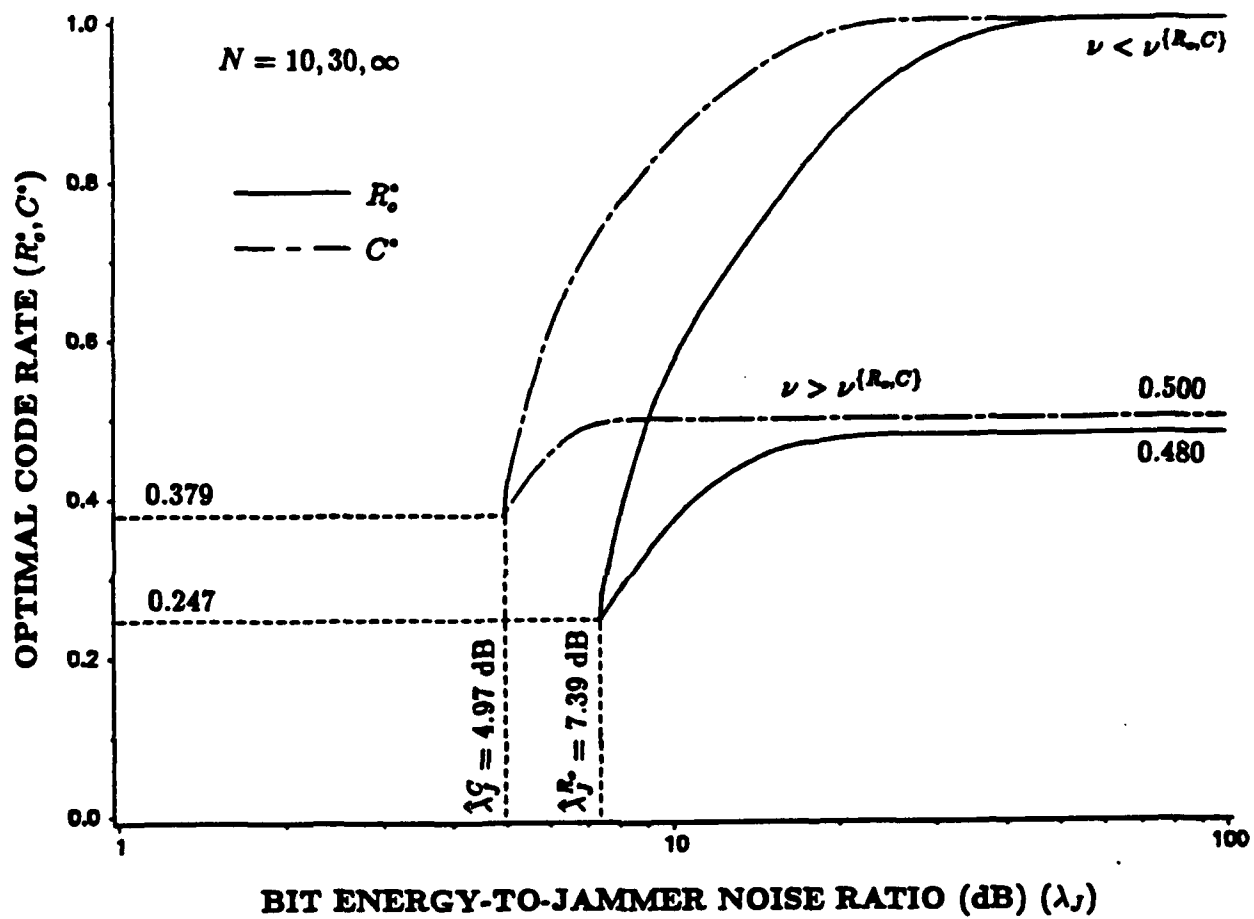


Figure 17: Optimal Code Rate versus Bit Energy-to-Jammer Noise Ratio  
(No Jammer State Information)



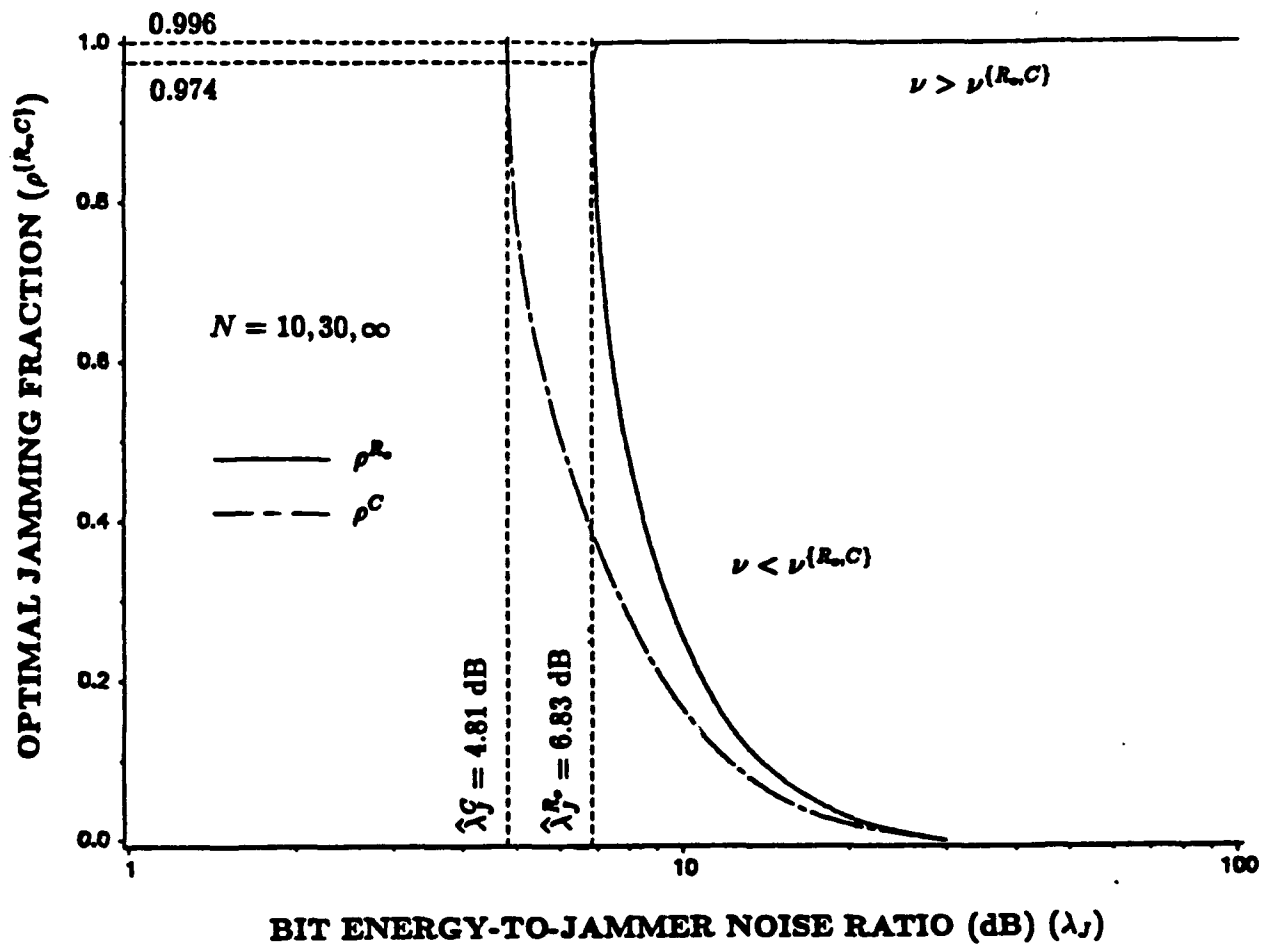


Figure 18: Optimal Jamming Fraction versus Bit Energy-to-Jammer Noise Ratio  
(Jammer State Information)

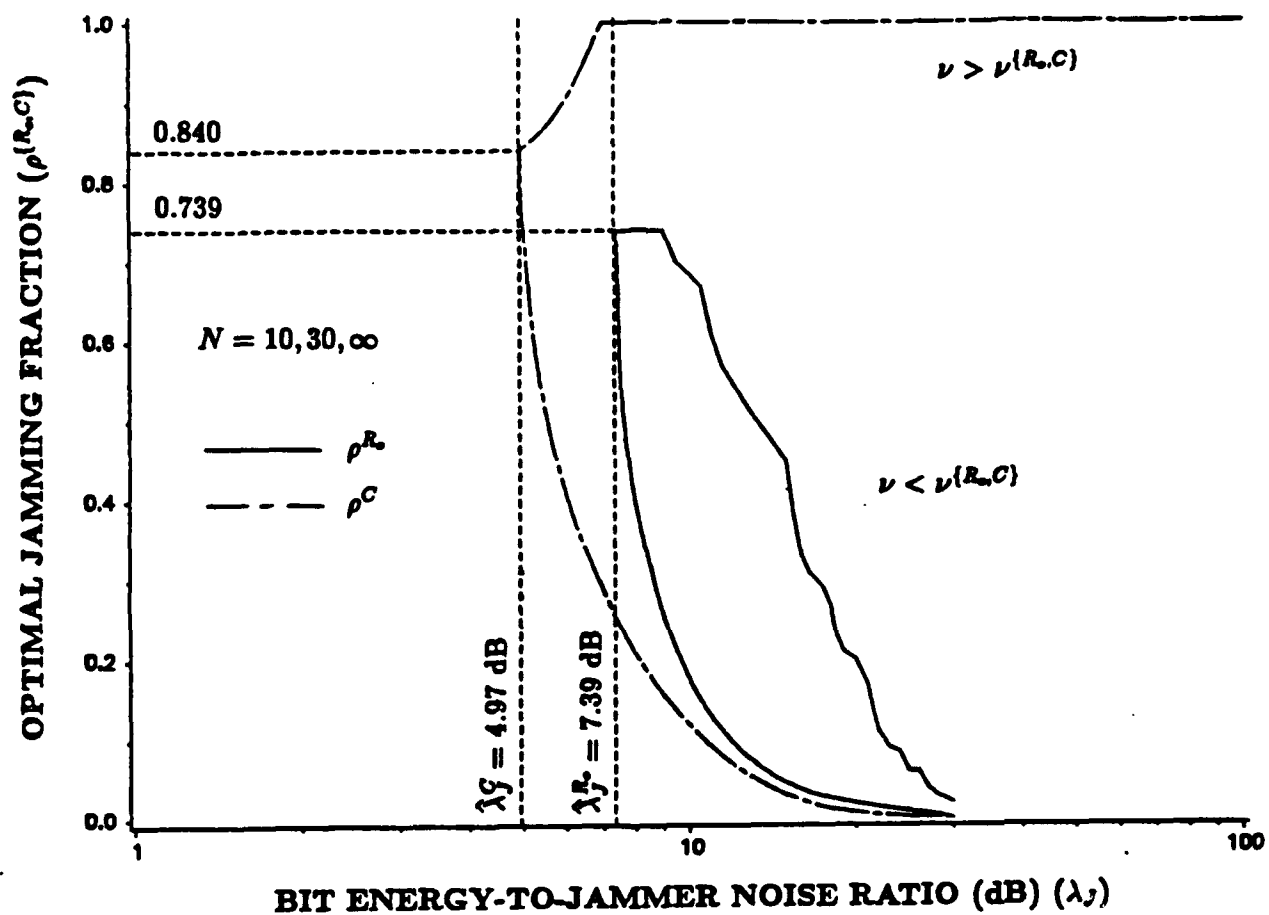


Figure 19: Optimal Jamming Fraction versus Bit Energy-to-Jammer Noise Ratio  
(No Jammer State Information)

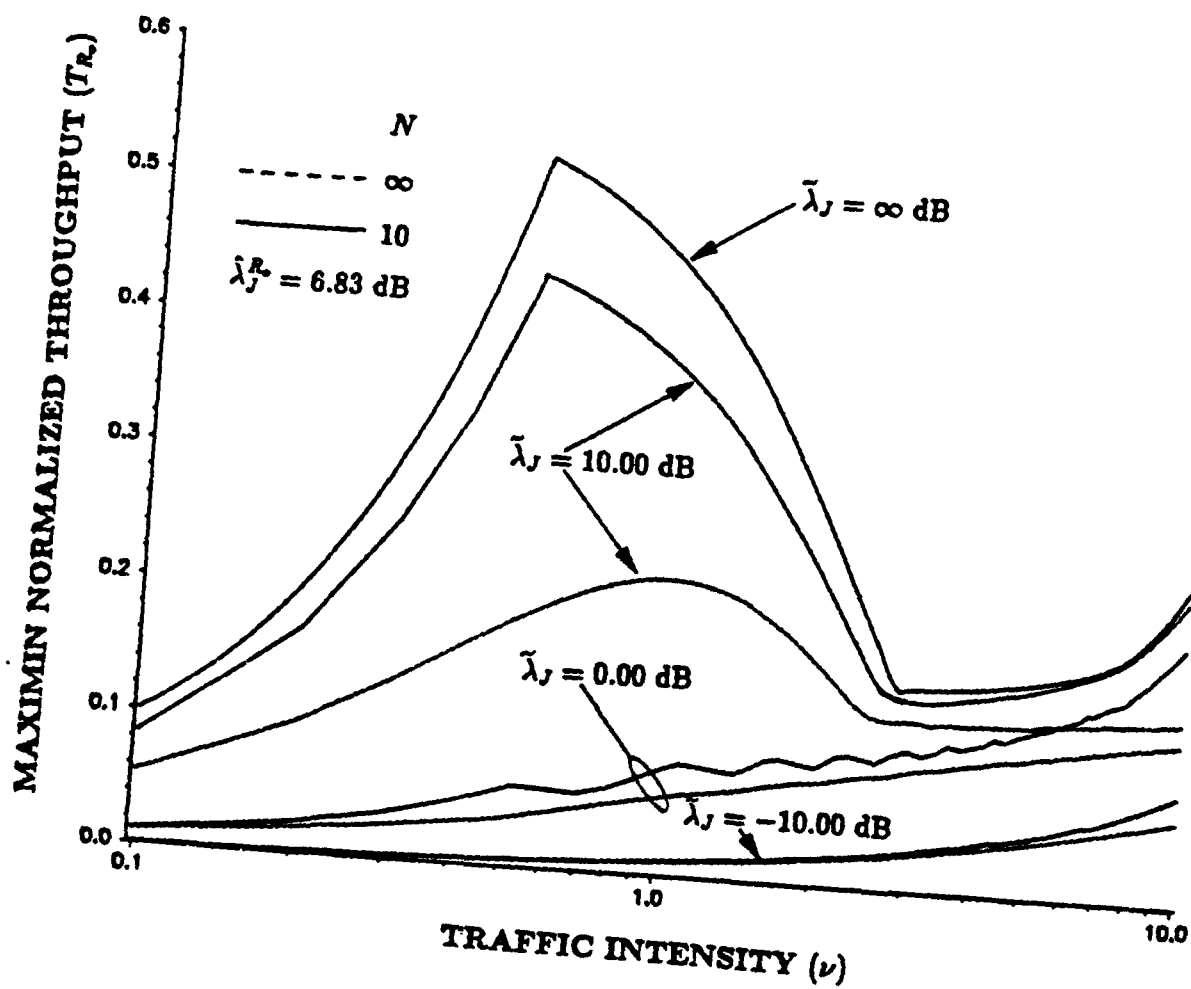


Figure 20: Maximin Normalized Throughput versus Traffic Intensity  
(Constant Jammer Power, Cutoff Rate Case, Jammer State Information)

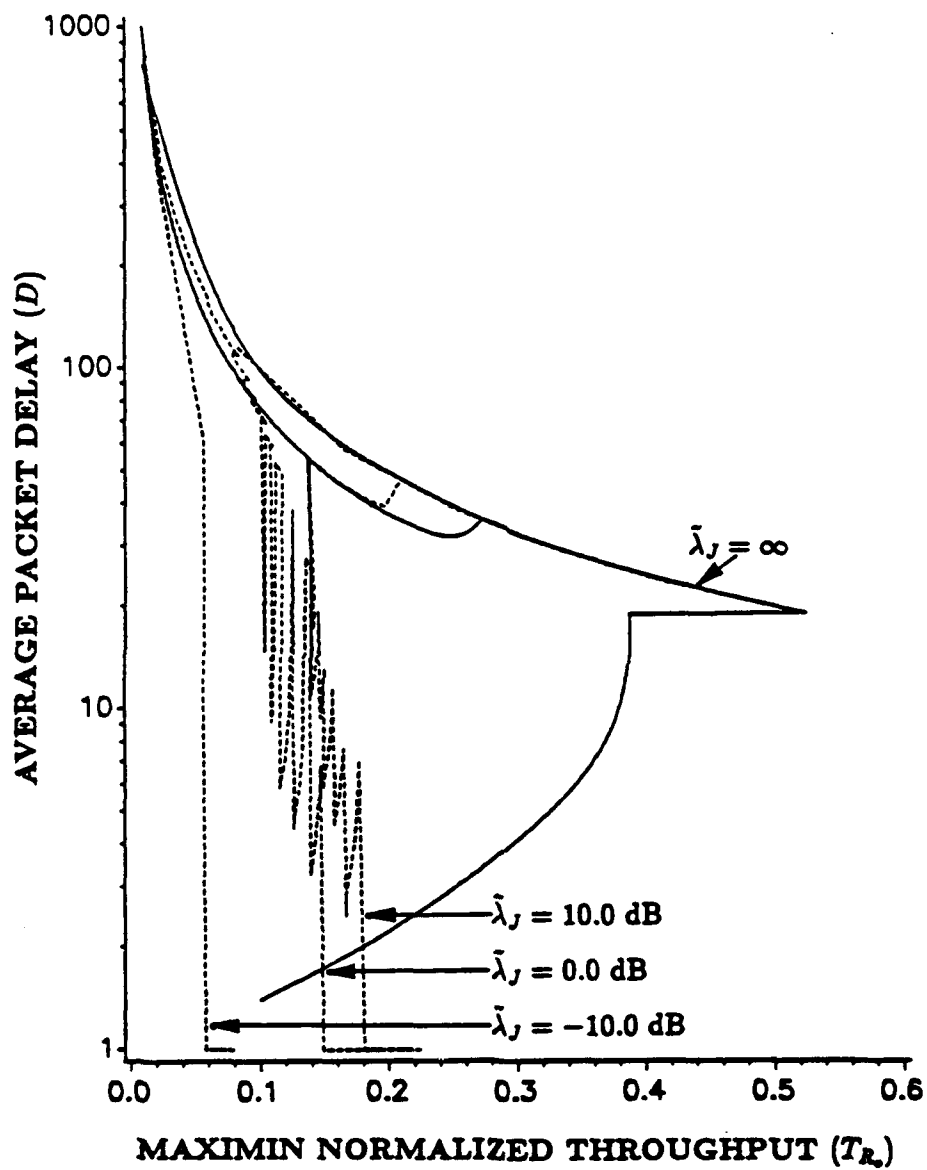


Figure 21: Average Packet Delay versus Maximin Normalized Throughput  
(Constant Jammer Power, Cutoff Rate Case, Jammer State Information)

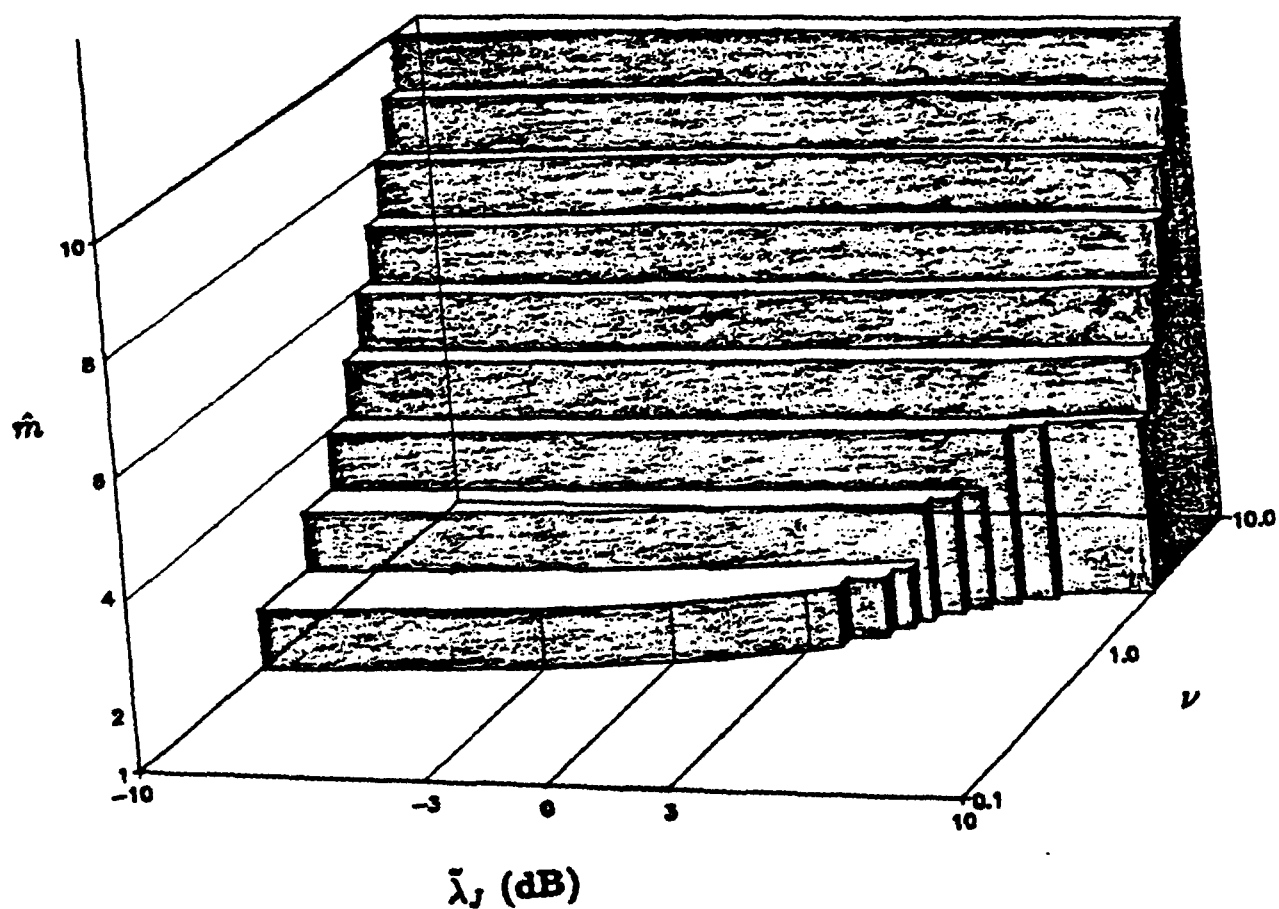


Figure 22: Number of Simultaneous Users ( $\hat{m}$ ) versus Traffic Intensity ( $\nu$ ) versus Bit Energy-to-Jammer Noise Ratio ( $\tilde{\lambda}_J$ ) for  $N = 10$   
(Constant Jammer Power, Cutoff Rate Case, Jammer State Information)

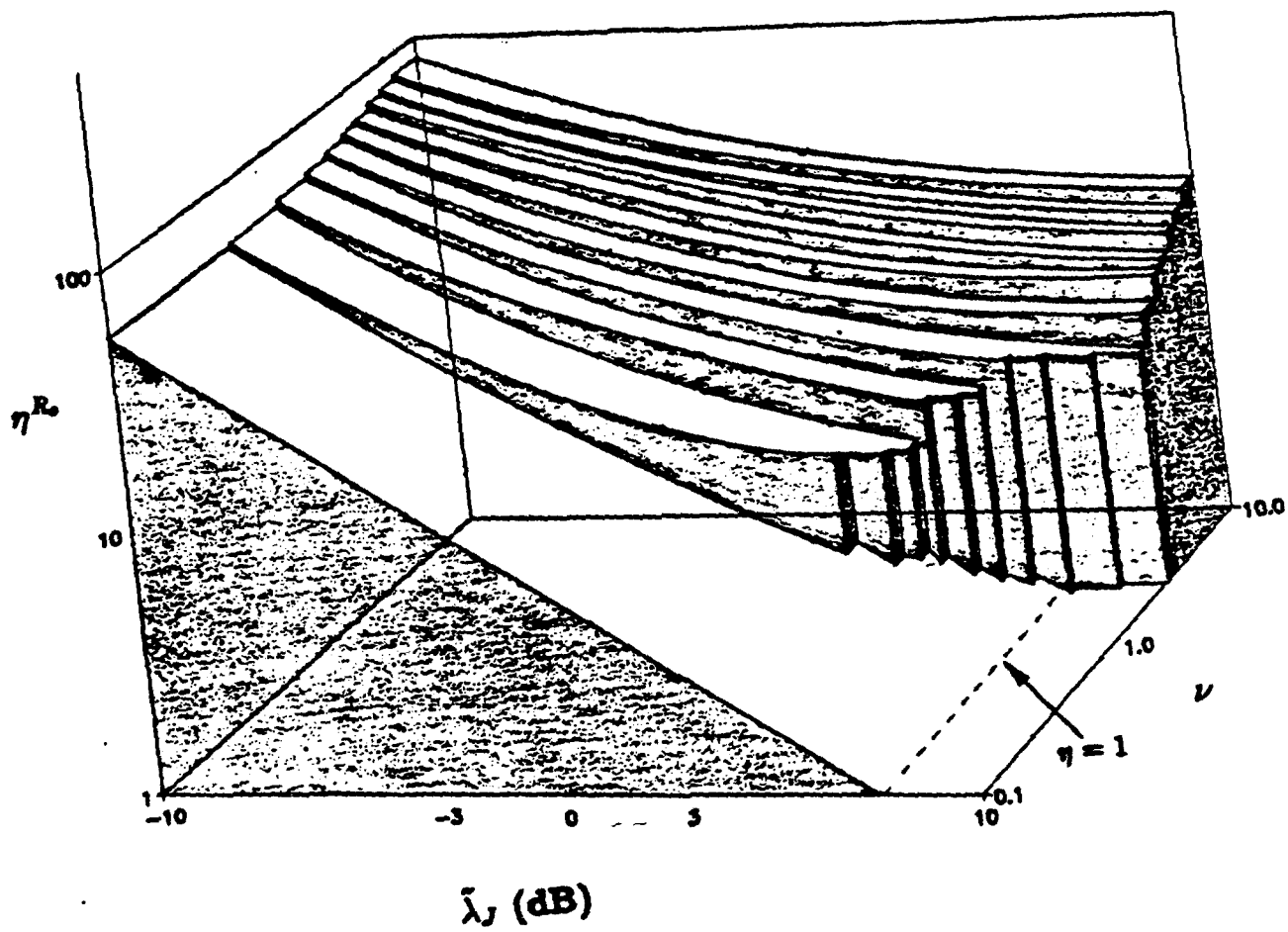


Figure 23: Optimal Processing Gain ( $\eta^{R_o}$ ) versus Traffic Intensity ( $\nu$ ) versus Bit Energy-to-Jammer Noise Ratio ( $\tilde{\lambda}_J$ ) for  $N = 10$   
(Constant Jammer Power, Cutoff Rate Case, Jammer State Information)

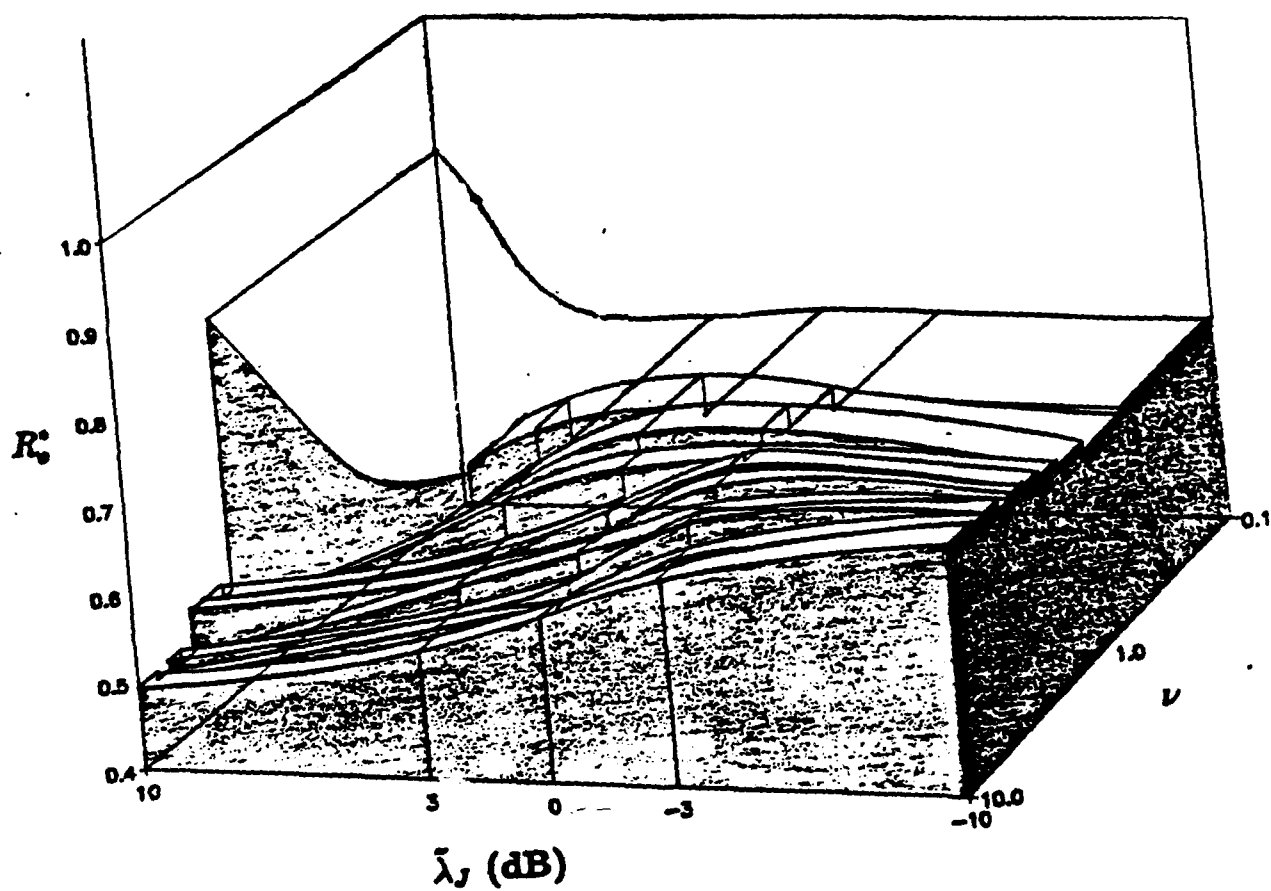


Figure 24: Optimal Code Rate ( $R_o^*$ ) versus Traffic Intensity ( $\nu$ ) versus Bit Energy-to-Jammer Noise Ratio ( $\tilde{\lambda}_J$ ) for  $N = 10$   
(Constant Jammer Power, Cutoff Rate Case, Jammer State Information)

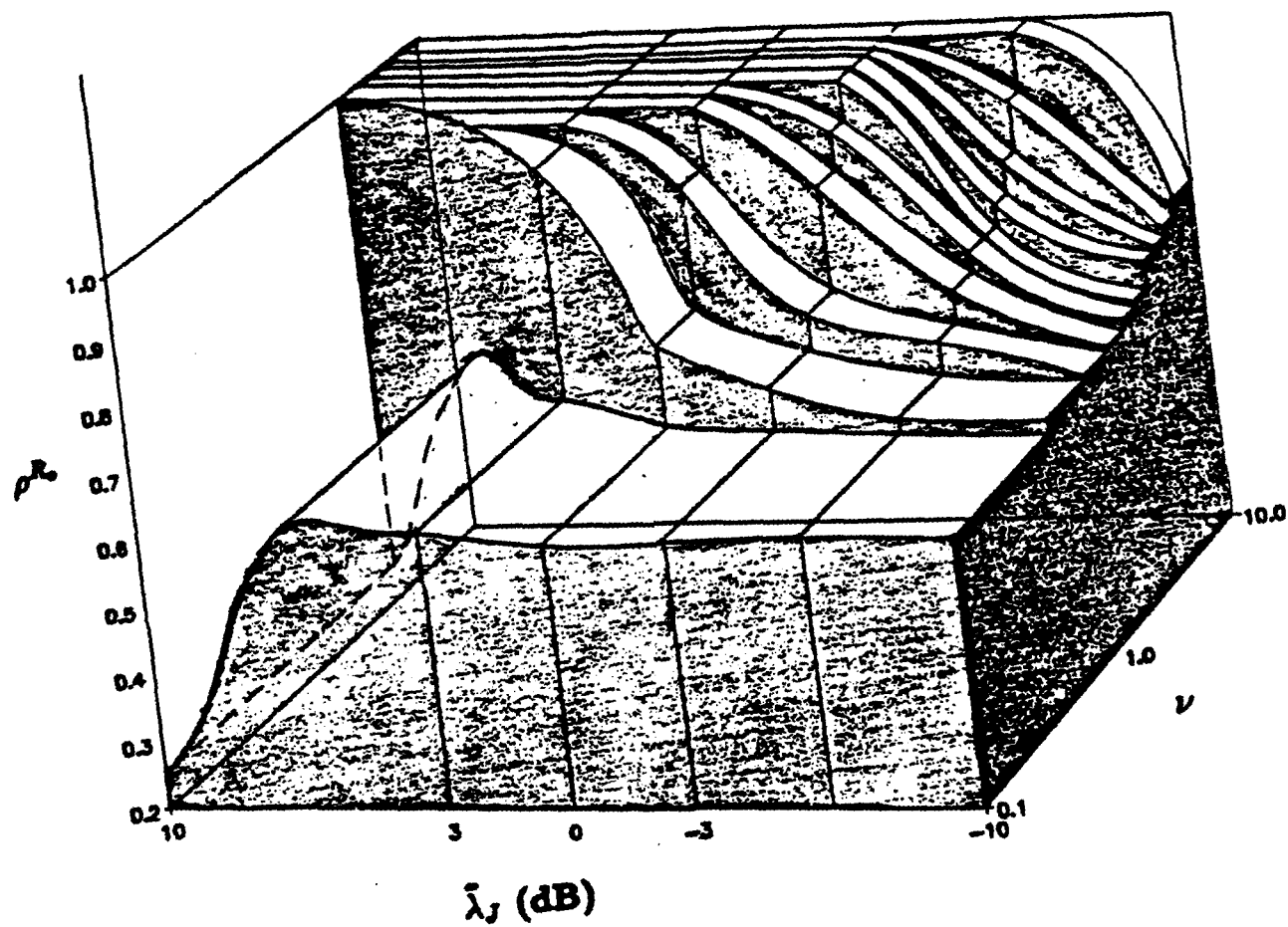


Figure 25: Optimal Jamming Fraction ( $\rho_{R^*}$ ) versus Traffic Intensity ( $\nu$ ) versus Bit Energy-to-Jammer Noise Ratio ( $\tilde{\lambda}_J$ ) for  $N = 10$   
(Constant Jammer Power, Cutoff Rate Case, Jammer State Information)



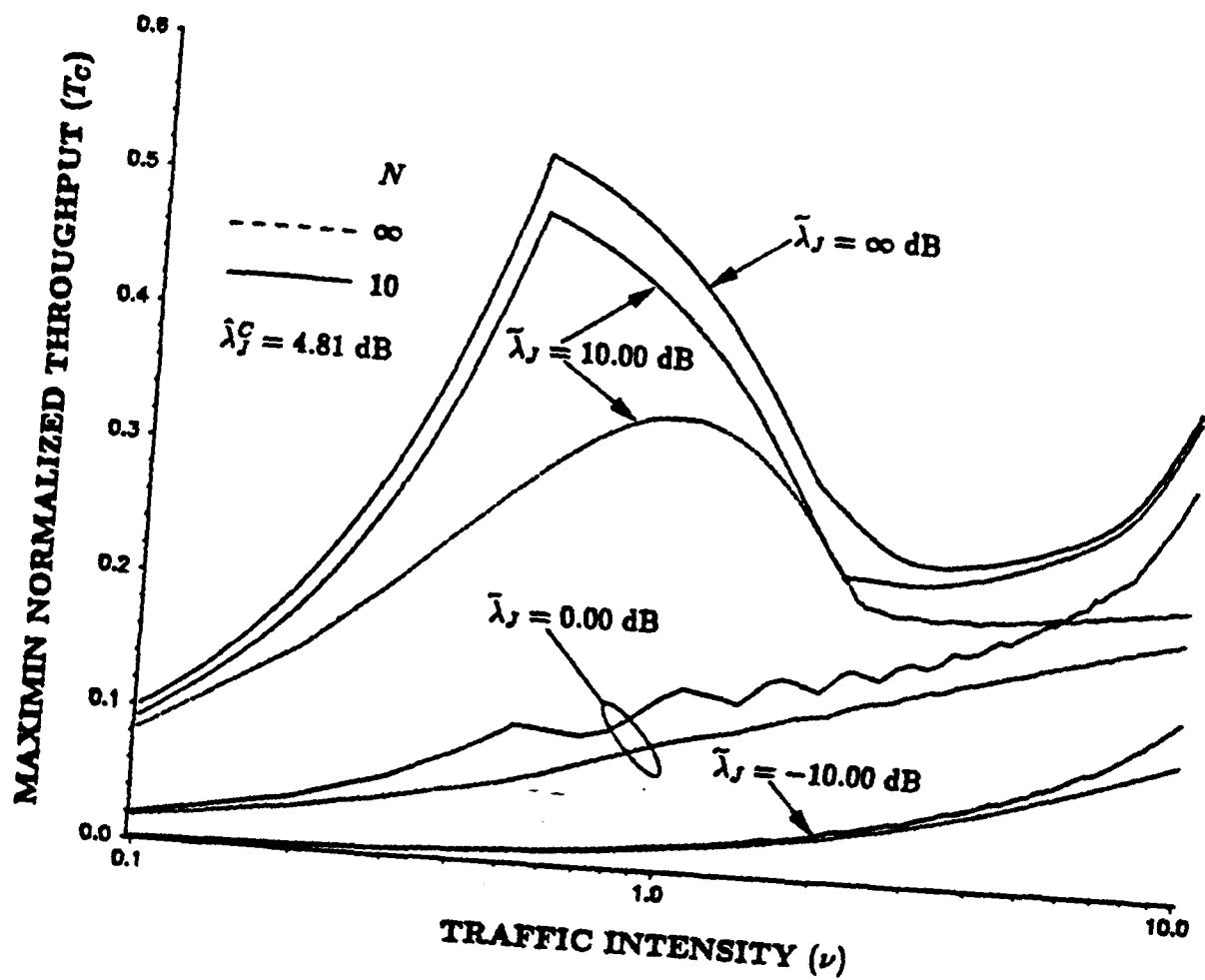


Figure 26: Maximin Normalized Throughput versus Traffic Intensity  
(Constant Jammer Power, Capacity Case, Jammer State Information)

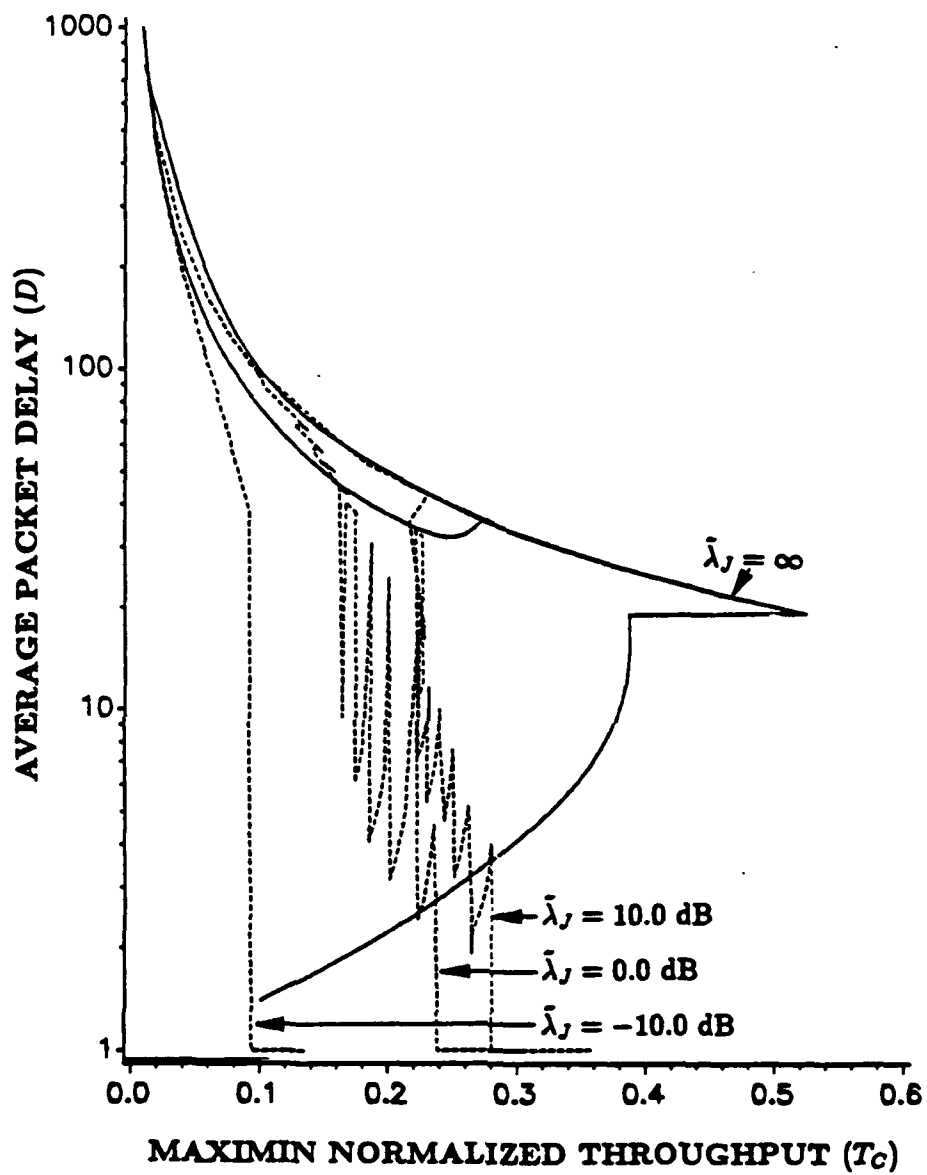


Figure 27: Average Packet Delay versus Maximin Normalized Throughput  
(Constant Jammer Power, Capacity Case, Jammer State Information)

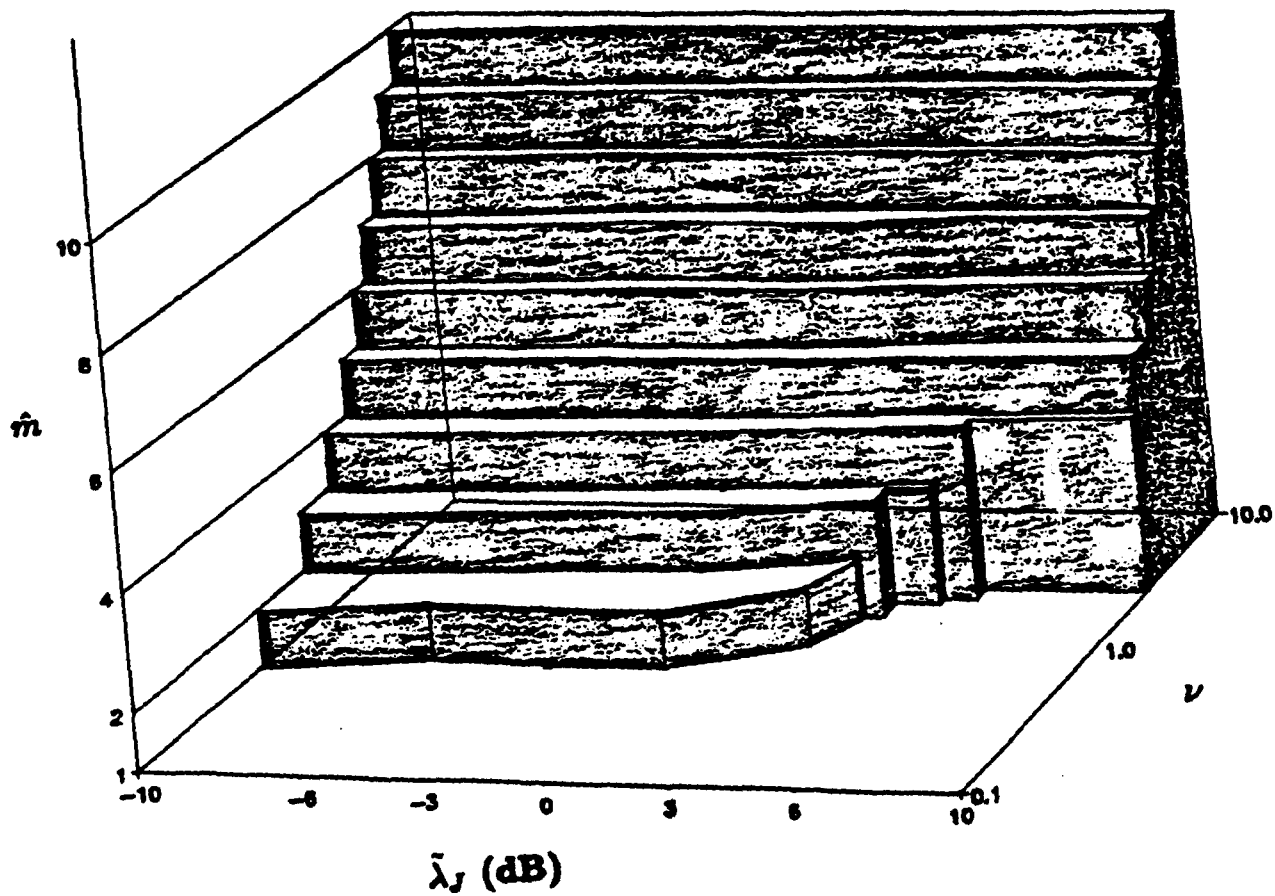


Figure 28: Number of Simultaneous Users ( $\hat{m}$ ) versus Traffic Intensity ( $\nu$ ) versus Bit Energy-to-Jammer Noise Ratio ( $\tilde{\lambda}_J$ ) for  $N = 10$   
(Constant Jammer Power, Capacity Case, Jammer State Information)

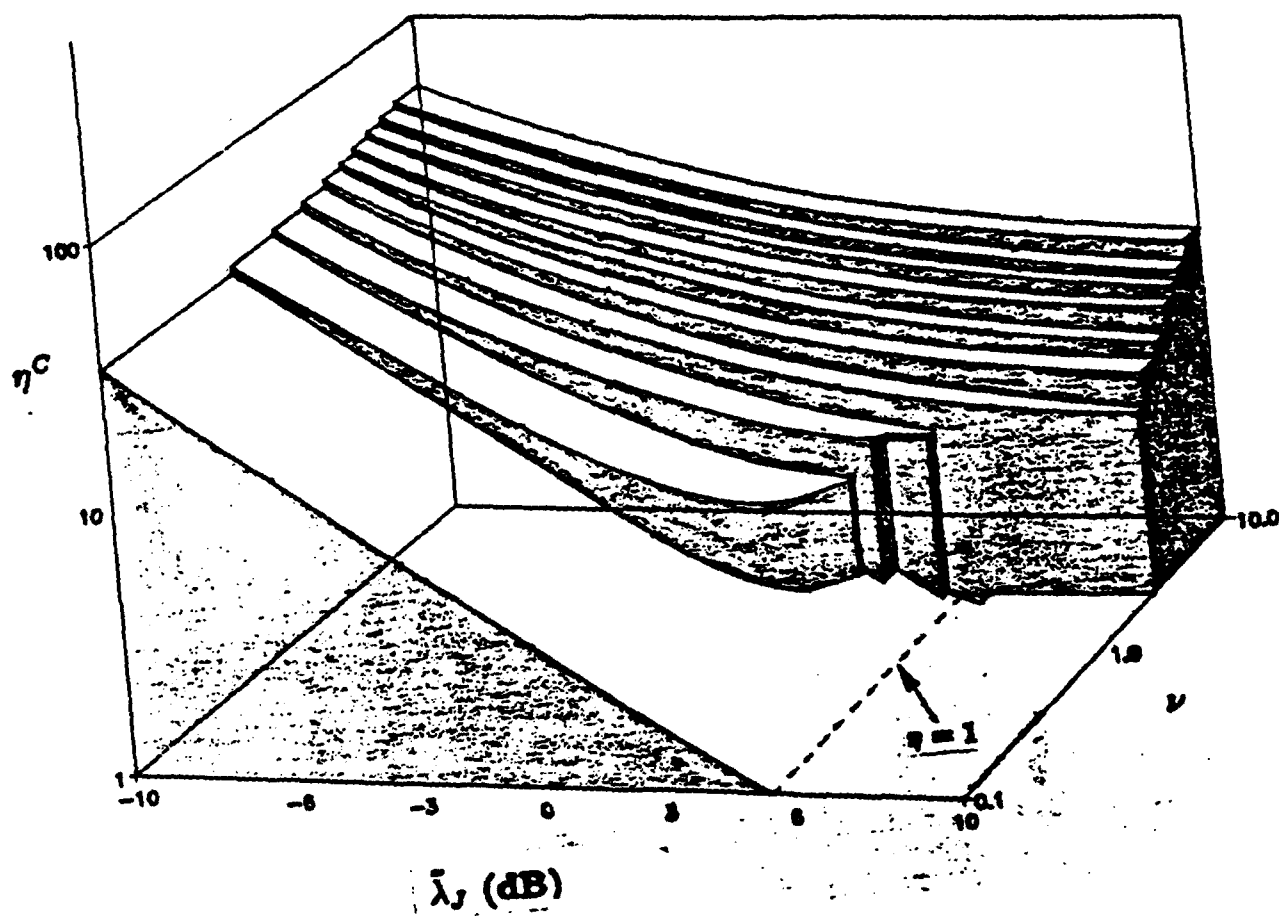


Figure 29: Optimal Processing Gain ( $\eta^C$ ) versus Traffic Intensity ( $\nu$ ) versus Bit Energy-to-Jammer Noise Ratio ( $\bar{\lambda}_J$ ) for  $N = 10$   
(Constant Jammer Power, Capacity Case, Jammer State Information)

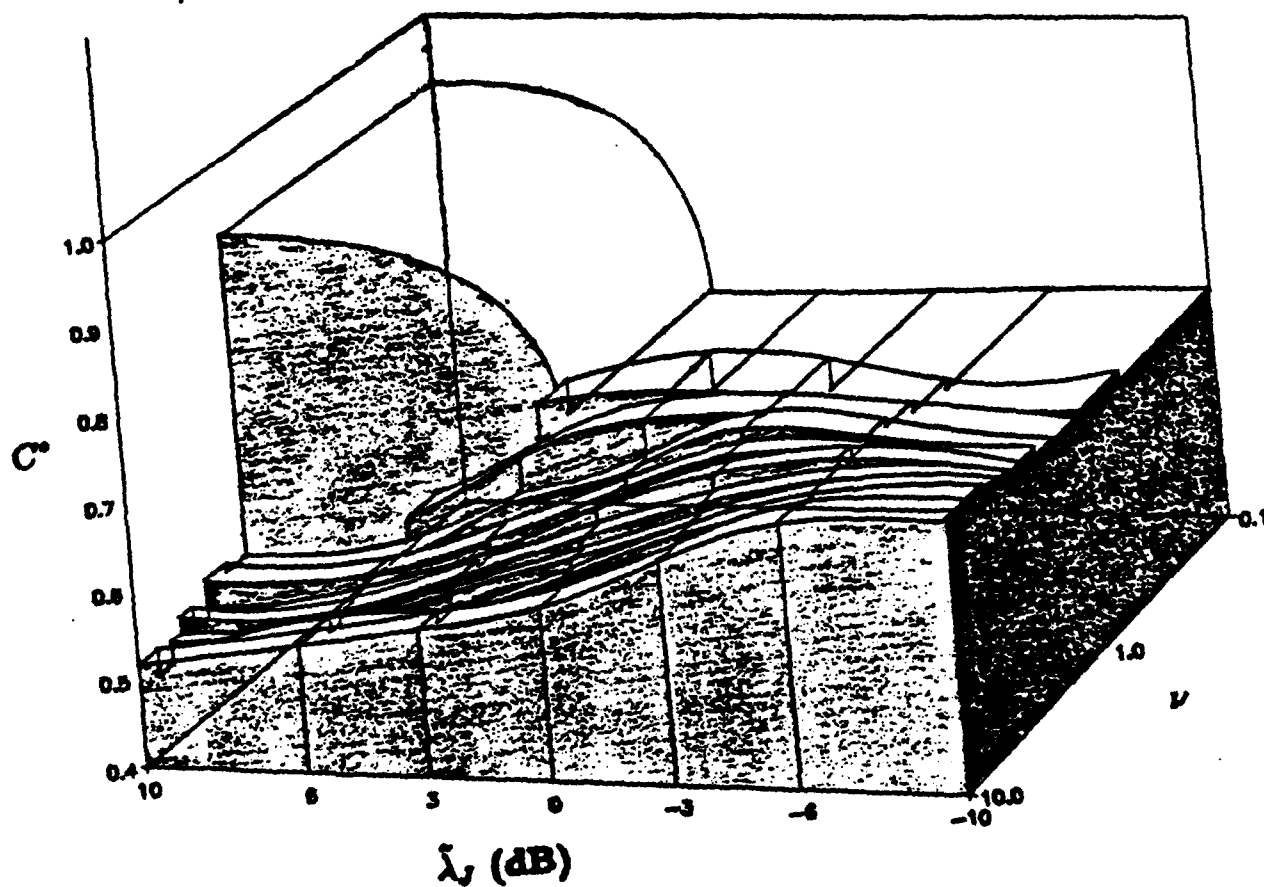


Figure 30: Optimal Code Rate ( $C^*$ ) versus Traffic Intensity ( $\nu$ ) versus Bit Energy-to-Jammer Noise Ratio ( $\tilde{\lambda}_J$ ) for  $N = 10$   
(Constant Jammer Power, Capacity Case, Jammer State Information)

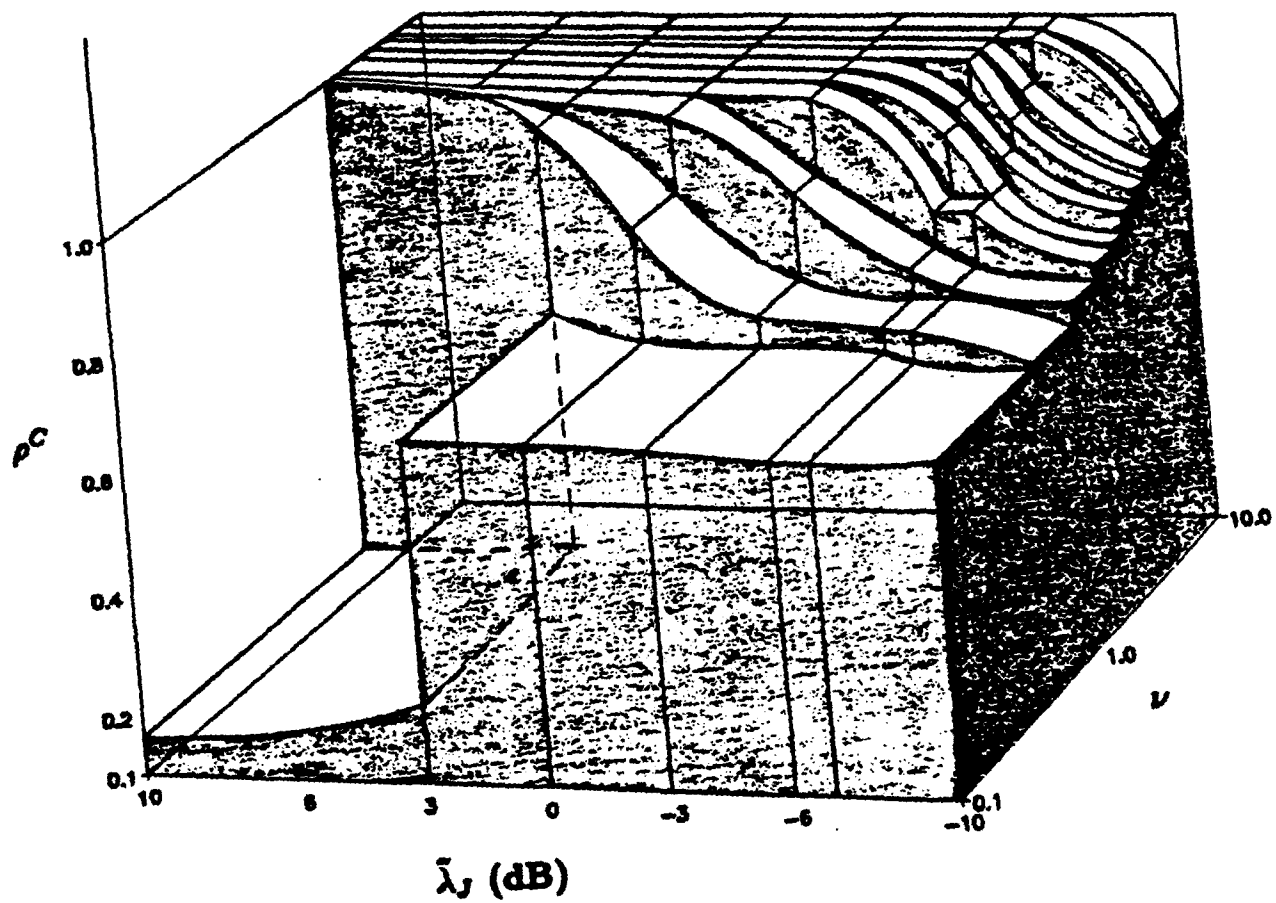


Figure 31: Optimal Jamming Fraction ( $\rho^C$ ) versus Traffic Intensity ( $\nu$ ) versus  
 Bit Energy-to-Jammer Noise Ratio ( $\tilde{\lambda}_J$ ) for  $N = 10$   
 (Constant Jammer Power, Capacity Case, Jammer State Information)

DEPARTMENT OF THE ARMY  
AIRMICS  
115 O'KEEFE BUILDING  
GEORGIA INSTITUTE OF TECHNOLOGY  
ATLANTA, GA 30332-0800

---

OFFICIAL BUSINESS  
PENALTY FOR PRIVATE USE, \$300

**THIRD CLASS**